RSC Advances

ROYAL SOCIETY OF CHEMISTRY

www.rsc.org/advances

Journal Name

RSCPublishing

ARTICLE

Relativistic effect on ^{125}Te and ^{33}S NMR chemical shifts of various tellurium and sulfur species, together with ^{77}Se of selenium congeners, in the framework of zeroth-order regular approximation: applicability to tellurium compounds†

Cite this: DOI: 10.1039/x0xx00000x

Received 0oth March 2014,
Accepted 0oth March 2014

DOI: 10.1039/x0xx00000x

www.rsc.org/

Satoko Hayashi, Kohei Matsuiwa and Waro Nakanishi*

The relativistic effect on absolute magnetic shielding tensors (σ(Z: Z = Te, Se and S)) are explicitly evaluated for various tellurium, selenium and sulfur species with the DFT(BLYP)-GIAO method. Calculations of σ(Te), σ(Se) and σ(S) are performed under the spin-orbit ZORA relativistic (Rlt-so) and nonrelativistic (Non) conditions with the Slater-type basis sets of the quadruple zeta all electron with four polarization functions (QZ4Pae). Structures optimized at the MP2 level under nonrelativistic conditions are employed for the evaluations. While the range of the relativistic effect on total shielding tensors for Te ($\Delta\sigma^t(Te)_{Rlt\text{-}so} = \sigma^t(Te)_{Rlt\text{-}so} - \sigma^{d+p}(Te)_{Non}$) is predicted to be −55 to 658 ppm, that for $\Delta\sigma^t(S)$ is 5 to 32 ppm, except for Me_2SBr_2 (TBP) of which $\Delta\sigma^t(S)_{Rlt\text{-}so} = -29$ ppm. The range for $\Delta\sigma^t(Se)$ is 2 to 153 ppm. The magnitudes of the relativistic effect on $\sigma^t(Te)$, $\sigma^t(Se)$ and $\sigma^t(S)$ are about 25 : 5 : 1. The applicability of $\sigma^t(Te)_{Rlt\text{-}so}$ to analyze $\delta(Te)_{obsd}$ is examined mainly at the OPBE//OPBE method under the spin-orbit ZORA relativistic conditions with QZ4Pae, in addition to above method.

Introduction

NMR spectroscopy has been established as a powerful tool to investigate molecular-level structures and dynamics in modern chemical sciences.[1] However, we often worry about the relativistic effect on NMR parameters for the better understanding of the observed values with the physical meanings. It is inevitable to take into account the relativistic effect[2] when absolute magnetic shielding tensors of nuclei N ($\sigma(N)$) are evaluated, especially for N of heavier atoms.[3,4] The relativistic effect on $\sigma(N)$[5,6] became to be evaluated successfully under the zeroth-order regular approximation (ZORA).[7] ZORA predicts more accurately for lower energy valence electrons than deep core states.[7a,8]

It is expected that the total values of $\sigma(N)$ ($\sigma^t(N)$) can be expressed as the sum of diamagnetic ($\sigma^d(N)$), paramagnetic ($\sigma^p(N)$) and spin-orbit ($\sigma^{so}(N)$) terms, as expressed in eq 1,[9] when evaluated considering the relativistic effect. The calculation conditions for $\sigma(N)$ are given just after $\sigma(N)$ as the subscript, in this paper. Therefore, $\sigma^t(N)_{Rlt\text{-}so}$ means the total values of $\sigma(N)$ calculated under the spin-orbit ZORA relativistic conditions (Rlt-so). The expectation shown in eq 1 will be rationalized when $\sigma^t(N)$ is evaluated under the Rlt-so conditions.

The framework of ZORA Hamiltonian is expressed by eq 2,[8] where $V(\boldsymbol{r})$ is the effective Kohn-Sham potential given by the sum of the nuclear, Hartree and exchange-correlation potentials in external magnetic field $\boldsymbol{B}$ within DFT (density functional theory), $\boldsymbol{\sigma}$ are the Pauli matrices, and c is the speed of light. $\boldsymbol{\pi}$ and $K(\boldsymbol{r})$ are given by eqs 3 and 4, respectively. The first two terms in eq 2 form the basis of the scalar relativistic approximation ($\sigma^{d+p}(N)$) and the third term represents spin-orbit coupling term ($\sigma^{so}(N)$). As a result, eq 1 is rationalized based on eq 2 by neglecting the forth term for the coupling between spin and magnetic field.

$$\sigma^t(N) = \sigma^d(N) + \sigma^p(N) + \sigma^{so}(N) = \sigma^{d+p}(N) + \sigma^{so}(N) \quad (1)$$

$$H_{ZORA} = V(\boldsymbol{r}) + \boldsymbol{\pi}(K(\boldsymbol{r})/2)\boldsymbol{\pi} + (K^2(\boldsymbol{r})/4c^2)\boldsymbol{\sigma}\bullet[\nabla V(\boldsymbol{r}) \times \boldsymbol{p}] - (K(\boldsymbol{r})/c)\boldsymbol{\sigma}\bullet\boldsymbol{p} \quad (2)$$

$$\boldsymbol{\pi} = \boldsymbol{p} + (1/c)\,\boldsymbol{A}(\boldsymbol{r});\ \boldsymbol{B} = \nabla\times\boldsymbol{A}(\boldsymbol{r}) \quad (3)$$

$$K(\boldsymbol{r}) = \{1 - (V(\boldsymbol{r})/2c^2)\}^{-1} \quad (4)$$

□□□□□ and ^{77}Se NMR parameters[10–12] are the typical cases for the relativistic effect to be considered. We reported the relativistic effect on σ(Se) evaluated explicitly and separately by the scalar ZORA and spin-orbit ZORA relativistic terms for various selenium species, employing the structures optimized at the B3LYP[13a,b] level under nonrelativistic conditions (Non)

($B3LYP_{Non}$), recently.[14] Observed NMR chemical shifts of Se ($\delta(Se)_{obsd}$) are well explained by $\sigma^t(Se)$, considering both scalar ZORA and spin-orbit ZORA relativistic terms. The scalar ZORA relativistic terms calculated under scalar ZORA relativistic conditions ($\sigma^{d+p}(Se)_{Rlt\text{-}sc}$) are very close to those calculated under spin-orbit ZORA relativistic conditions ($\sigma^{d+p}(Se)_{Rlt\text{-}so}$), although spin-orbit ZORA relativistic terms ($\sigma^{so}(Se)_{Rlt\text{-}so}$) can only be obtained under the Rlt-so conditions. Therefore, the effect evaluated under the Rlt-so conditions will be employed for the discussion.

The magnitudes of the relativistic effect are evaluated as the differences from the corresponding values calculated under nonrelativistic conditions ($\Delta\sigma(Se)_{Rlt} = \sigma(Se)_{Rlt} - \sigma(Se)_{Non}$). The relativistic effect on σ(Se) of the scalar ZORA and spin-orbit ZORA relativistic terms, calculated under the Rlt-so conditions, are abbreviated as $\Delta\sigma^{d+p}(Se)_{Rlt\text{-}so}$ (= $\sigma^{d+p}(Se)_{Rlt\text{-}so} - \sigma^{d+p}(Se)_{Non}$) and $\sigma^{so}(Se)_{Rlt\text{-}so}$, respectively. The values were reported to be –127 to –26 ppm (downfield) and 95 to 221 ppm (upfield), respectively, and the effect on $\sigma^t(Se)$ ($\Delta\sigma^t(Se)_{Rlt\text{-}so} = \Delta\sigma^{d+p}(Se)_{Rlt\text{-}so} + \sigma^{so}(Se)_{Rlt\text{-}so}$) was determined to be 2 to 153 ppm for various selenium species (40 species) under the Rlt-so conditions.[14] It is worthwhile to comment that $\sigma^{so}(Se)_{Rlt\text{-}so}$ should be contained when $\delta(Se)_{obsd}$ is analyzed considering the relativistic effect, since $\sigma^{d+p}(Se)_{Rlt\text{-}so}$ would not improve the applicability of σ(Se) so much to analyze $\delta(Se)_{obsd}$. Indeed, $\sigma^{d+p}(Se)_{Non}$ often reproduce $\delta(Se)_{obsd}$ better than the case of $\sigma^{d+p}(Se)_{Rlt\text{-}so}$. Physical meanings of $\delta(Se)_{obsd}$ should also be explained by considering both scalar ZORA and spin-orbit ZORA relativistic effect.

How is the relativistic effect on σ(Te) and σ(S)? The effect on σ(S) would be negligibly smaller, whereas that on σ(Te)[15] must be much larger, relative to the case of σ(Se).[14] It must also be of highly interest to discuss the trends of the effect on σ(Te), σ(Se) and σ(S) as the group 16 elements. $\delta(Te)_{obsd}$ are reported to be proportional to $\delta(Se)_{obsd}$ when the values of structurally equivalent compounds are compared. This may show the existence of some linear correlations between σ(Te) and σ(Se) not only for those evaluated under nonrelativistic conditions but also under relativistic conditions.

Here, we present the results of calculations of the relativistic effect on σ(Z) and the components, $\sigma^d(Z)$, $\sigma^p(Z)$, $\sigma^{d+p}(Z)$, $\sigma^{so}(Z)$ and $\sigma^t(Z)$ (Z = Te and S), for various tellurium and sulfur species (40 species for each of Z), together with the Se derivatives. The values are evaluated explicitly and separately by the scalar ZORA and spin-orbit ZORA relativistic terms. The calculation method for σ(Te) and σ(S) is set up equal to that for σ(Se),[14] for convenience of comparison. Trends of the effect on σ(Te), σ(Se) and σ(S) are also discussed. The applicability of $\sigma^t(Te)_{Rlt\text{-}so}$ to analyze $\delta(Te)_{obsd}$ is examined carefully employing $\sigma^t(Te)_{Rlt\text{-}so}$ of 46 organic tellurium species (almost other than above 40), calculated similarly at the OPBE level under the Rlt-so conditions on the optimized structures with the same method ($OPBE_{Rlt\text{-}so}$//$OPBE_{Rlt\text{-}so}$), in addition to those with $BLYP_{Rlt\text{-}so}$//$OPBE_{Rlt\text{-}so}$ and $BLYP_{Rlt\text{-}so}$//$MP2_{Non}$.

The relativistic effect on σ(Z: Z = Te and S) will be discussed employing $\Delta\sigma(Z)_{Rlt\text{-}so}$ (= $\sigma(Z)_{Rlt\text{-}so} - \sigma(Z)_{Non}$), similarly to the case of Z = Se. The $\Delta\sigma(Z)_{Rlt\text{-}so}$ values are analyzed by decomposing the contributions into $\Delta\sigma^d(Z)_{Rlt\text{-}so}$ (= $\sigma^d(Z)_{Rlt\text{-}so} - \sigma^d(Z)_{Non}$), $\Delta\sigma^p(Z)_{Rlt\text{-}so}$ (= $\sigma^p(Z)_{Rlt\text{-}so} - \sigma^p(Z)_{Non}$), $\Delta\sigma^{d+p}(Z)_{Rlt\text{-}so}$ (= $\sigma^{d+p}(Z)_{Rlt\text{-}so} - \sigma^{d+p}(Z)_{Non} = \Delta\sigma^d(Z)_{Rlt\text{-}so} + \Delta\sigma^p(Z)_{Rlt\text{-}so}$), $\sigma^{so}(Z)_{Rlt\text{-}so}$ and $\Delta\sigma^t(Z)_{Rlt\text{-}so}$ (= $\sigma^t(Z)_{Rlt\text{-}so} - \sigma^{d+p}(Z)_{Non} = \Delta\sigma^{d+p}(Z)_{Rlt\text{-}so} + \sigma^{so}(Z)_{Rlt\text{-}so}$), according to eq 1. The first three terms correspond to the diamagnetic, paramagnetic and (diamagnetic + paramagnetic) terms of the relativistic effect on σ(Z), where $\sigma(Z)_{Rlt\text{-}so}$ shows the values being calculated under the Rlt-so conditions. $\sigma^{so}(Z)_{Rlt\text{-}so}$ is the spin-orbit ZORA relativistic term, which can only be calculated under the Rlt-so conditions. The symbols and definitions for σ(Z: Z = Te, Se and S) and Δσ(Z: Z = Te, Se and S) used in this paper and the previous one,[14] evaluated under the Non, Rlt-sc and Rlt-so conditions, are listed in Table S1 of the Supporting Information. Indeed, $\sigma^{d+p}(Z)_{Rlt\text{-}sc}$ and $\Delta\sigma^{d+p}(Z)_{Rlt\text{-}sc}$ correspond to $\sigma^t(Z)_{Rlt\text{-}sc}$ and $\Delta\sigma^t(Z)_{Rlt\text{-}sc}$, respectively, if evaluated at the Rlt-sc level, but they will not be denoted as the latter, in this series of investigations. $\sigma^t(Z)_{Rlt\text{-}so}$ and $\Delta\sigma^t(Z)_{Rlt\text{-}so}$ will be used only for the total values calculated at the Rlt-so level.

Calculation Method

The σ(Z) ($\sigma^d(Z)$, $\sigma^p(Z)$, $\sigma^{so}(Z)$ and $\sigma^t(Z)$ (Z = Te, Se and S) values are calculated under relativistic and nonrelativistic conditions for various species containing tellurium and sulfur (() species for each). The calculation method for σ(Te) and σ(S) is set up equal to that for σ(Se), reported recently.[14] The ADF 2013 program[16-18] is employed for the calculations. The GIAO (Gauge-Independent Atomic Orbital) method[19] is applied to evaluate σ(Z: Z = Te, Se and S) at the DFT level of the Becke density functional with the Lee–Yang–Parr correlation functional (BLYP)[13b,c] (the DFT(BLYP)-GIAO method). Calculations of σ(Se) are performed at the BLYP level under the Non and Rlt-so conditions ($BLYP_{Non}$ and $BLYP_{Rlt\text{-}so}$, respectively). The Slater-type basis sets of quadruple zeta all-electron with four polarization functions (QZ4Pae: 3×1s, 3×2s, 3×2p, 5×3s, 4×3p, 3×3d and 2×4f for S, 4×1s, 3×2s, 4×2p, 3×3s, 3×3p, 4×3d, 4×4s, 4×4p, 2×4d and 3×4f for Se and 5×1s, 3×2s, 5×2p, 3×3s, 3×3p, 3×3d, 3×4s, 3×4p, 4×4d, 3×4f, 4×5s, 4×5p and 1×5d for Te) are applied for the calculations.[20,21] The relativistic effect on $\sigma^t(Z)$ is analyzed separately by $\sigma^d(Z)$, $\sigma^p(Z)$, $\sigma^{d+p}(Z)$, and $\sigma^{so}(Z)$. The σ(S) values are given without scaling (*cf*: EMPI approach[22]).

The structures of tellurium, selenium and sulfur species are optimized using the Gaussian 03 program package,[23] of which NMR parameters are given in Table 1, Tables S2-S6, Figures 1-3 and Figures S1-S3. The (7433111/743111/7411/2 + 1s1p1d1f) type basis set[24] is employed for Te with the 6-311+G(3df,3pd) type[25] for other nuclei in the optimizations (the all-electron basis set system). The optimizations are performed at the Møller-Plesset second-order energy correlation (MP2) level[20,21] and the DFT (B3LYP)[13a,b] level under the Non conditions ($MP2_{Non}$ and $B3LYP_{Non}$, respectively). Calculations of σ(Z: Z = Te, Se and S) are unsuccessful for a few structures, maybe due to some problem in the integration processes. In

such cases, the processes can be successful by employing the structures of lower symmetry. The relativistic effect on σ(Z: Z = Te, Se and S) are mainly discussed calculated employing the optimized structures at the $MP2_{Non}$ level.

To examine the applicability of $\sigma^{t}(Te)_{Rlt\text{-}so}$ to analyze $\delta(Te)_{obsd}$, $\sigma^{t}(Te)_{Rlt\text{-}so}$, together with $\sigma^{d+p}(Te)_{Rlt\text{-}so}$ and $\sigma^{so}(Te)_{Rlt\text{-}so}$, are evaluated similarly at the OPBE level under the spin-orbit ZORA relativistic conditions using the optimized structures with the same method ($OPBE_{Rlt\text{-}so}$//$OPBE_{Rlt\text{-}so}$) for 46 tellurium species, almost other than above 40. The values are also calculated at the BLYP level under the spin-orbit ZORA relativistic conditions using the optimized structures at the $OPBE_{Rlt\text{-}so}$ and $MP2_{Non}$ levels for the 46 tellurium species ($BLYP_{Rlt\text{-}so}$//$OPBE_{Rlt\text{-}so}$ and $BLYP_{Rlt\text{-}so}$//$MP2_{Non}$, respectively). The $\sigma^{d+p}(Te)_{Non}$ values are also calculated with the $OPBE_{Non}$//$OPBE_{Rlt\text{-}so}$ and $BLYP_{Non}$//$MP2_{Non}$ methods for convenience of comparison. Partial optimizations at the $OPBE_{Non}$ level are applied to obtain the structures having the observed bond length(s) around Te in some tellurium compounds to examine the applicability in more detail.

Results and Discussion

Relativistic Effect on σ(Te), σ(Se), and σ(S) Evaluated with the QZ4Pae Basis Sets

Table 1 collects $\sigma^{d}(Te)_{Rlt\text{-}so}$, $\sigma^{p}(Te)_{Rlt\text{-}so}$, $\sigma^{d+p}(Te)_{Rlt\text{-}so}$, $\sigma^{so}(Te)_{Rlt\text{-}so}$ and $\sigma^{t}(Te)_{Rlt\text{-}so}$ calculated under the Rlt-so conditions with QZ4Pae, employing the structures optimized at the $MP2_{Non}$ level. Table 1 also contains $\sigma^{d}(Te)_{Non}$, $\sigma^{p}(Te)_{Non}$ and $\sigma^{d+p}(Te)_{Non}$ obtained similarly under the Non conditions. Data for σ(Se) and σ(S) calculated under the Rlt-so conditions with QZ4Pae, employing the structures similarly optimized at the $MP2_{Non}$ level, are summarized in Tables S2 and S3, respectively, of the Supporting Information. Those for σ(Te), σ(Se) and σ(S) evaluated similarly, employing the structures optimized at the $B3LYP_{Non}$ level are given in Tables S4–S6, respectively, of the Supporting Information, for convenience of comparison.

Before discussion of the effect on each term, the relativistic effect on σ(Z) are overviewed. As shown in Table 1, the range for $\Delta\sigma^{d+p}(Te)_{Rlt\text{-}so}$ is evaluated to be –459 to –110 ppm (downfield shifts), whereas that for $\sigma^{so}(Te)_{Rlt\text{-}so}$ is 331 to 889 ppm (upfield shifts) for the Te species. Consequently, the range for $\Delta\sigma^{t}(Te)_{Rlt\text{-}so}$ is predicted to be –55 to 658 ppm. Figure 1 plots the data for $\Delta\sigma^{d+p}(Te)_{Rlt\text{-}so}$, $\sigma^{so}(Te)_{Rlt\text{-}so}$ and $\Delta\sigma^{t}(Te)_{Rlt\text{-}so}$ given in Table 1. On the other hand, ranges for $\Delta\sigma^{d+p}(Se)_{Rlt\text{-}so}$, $\sigma^{so}(Se)_{Rlt\text{-}so}$ and $\Delta\sigma^{t}(Se)_{Rlt\text{-}so}$ are evaluated to be –127 to –26 ppm, 95 to 221 ppm and 2 to 153 ppm, respectively, as shown in Table S2. Figure 2 summarizes the $\Delta\sigma^{d+p}(Se)_{Rlt\text{-}so}$, $\sigma^{so}(Se)_{Rlt\text{-}so}$ and $\Delta\sigma^{t}(Se)_{Rlt\text{-}so}$ values.

In the case of σ(S), the ranges for $\Delta\sigma^{d+p}(S)_{Rlt\text{-}so}$, $\sigma^{so}(S)_{Rlt\text{-}so}$ and $\Delta\sigma^{t}(S)_{Rlt\text{-}so}$ are evaluated to be –12 to 1 ppm, 11 to 38 ppm and 5 to 32 ppm, except for Me_2SBr_2 (C_{2v}). The values for Me_2SBr_2 (C_{2v}) are –8.6, –19.9 and –28.6 ppm, respectively. While the $\Delta\sigma^{d+p}(S)_{Rlt\text{-}so}$ value drops in the range, $\sigma^{so}(S)_{Rlt\text{-}so}$ and $\Delta\sigma^{t}(S)_{Rlt\text{-}so}$ seem smaller than the ranges by around 45 ppm, which would be the reflection of the second relativistic effect from heavier Br atoms. Figure 3 summarizes the data for $\Delta\sigma^{d+p}(S)_{Rlt\text{-}so}$, $\sigma^{so}(S)_{Rlt\text{-}so}$ and $\Delta\sigma^{t}(S)_{Rlt\text{-}so}$, of which values are given in Table S3. The relativistic effect on σ(S) is small, therefore, it could be neglected for usual purpose of analysis, although we must be careful when heavier atoms are attached to the atom. Relative ranges of the relativistic effect on $\sigma^{t}(S)_{Rlt\text{-}so}$, $\sigma^{t}(Se)_{Rlt\text{-}so}$, □□□□$\sigma^{t}(Te)_{Rlt\text{-}so}$ are around 1 : 5 : 25.

The relativistic effect on each term of σ(Te) is discussed next. The effect on $\sigma^{d}(Te)$ causes small downfield shifts under the Rlt-so conditions. The $\Delta\sigma^{d}(Te)_{Rlt\text{-}so}$ values are almost constant, which are –58.0 ± 3.7 ppm for the species in Table 1. The magnitudes are about 2.6 and 9.8 times larger than those of $\Delta\sigma^{d}(Se)_{Rlt\text{-}so}$ (–22.2 ± 2.0 ppm) and $\Delta\sigma^{d}(S)_{Rlt\text{-}so}$ (–5.9 ± 4.4 ppm), respectively. The relativistic effect on $\sigma^{d}(Te)$, $\sigma^{d}(Se)$ and $\Delta\sigma^{d}(S)$ could be almost entirely neglected when the relative values from a standard compound, such as MeZMe, ($\sigma^{d}(Z: Z = Te, Se and S)_{r}$) are employed for analysis.

The plot of $\sigma^{p}(Te)_{Rlt\text{-}so}$ versus $\sigma^{p}(Te)_{Non}$ gave a very good correlation, although data for MeTeTeMe seem to deviate slightly to the downside of the correlation line. The plot is shown in Figure S4. The plot is analyzed as the linear correlation with $y = ax + b$, where a and b are the correlation constant and the y-intercept, respectively, with the square of correlation coefficient, R^2. The correlation is given in entries 1 and 1' of Table 2 for all data and data without those of MeTeTeMe, respectively. The a values are very close to 1.10. The a values larger than 1.00 must be the reflection of larger downfield contributions from the relativistic effect on $\sigma^{p}(Te)$ for higher coordinated tellurium species, as a whole.

How do $\Delta\sigma^{p}(Te)_{Rlt\text{-}so}$ behave? $\Delta\sigma^{p}(Te)_{Rlt\text{-}so}$ are plotted versus $\sigma^{p}(Te)_{Non}$. Figure 4 shows the results. The plot is analyzed as three (linear) correlations, although tentative. The first group contains mono- and di-coordinated Te species, R_3Te^{+} and R_4Te (R = H and Me) form the second group, and the Te species in Table 1 other than the first and second groups belong to the third group. The correlations are given in the Figure. The relativistic effect on $\sigma^{p}(Te)$ of MeTeTeMe (σ^{p}(Te: MeTeTeMe)$_{Rlt\text{-}so}$) shifts more downfield by ca 190 ppm than that expected from σ^{p}(Te: MeTeTeMe)$_{Non}$ of –2736 ppm. The results are similar to those predicted for $\Delta\sigma^{p}(Se)_{Rlt\text{-}so}$, although the plot of $\Delta\sigma^{p}(Se)_{Rlt\text{-}so}$ versus $\sigma^{p}(Se)_{Non}$ is analyzed assuming a cubic function.[14] The results anticipate us the linear relation in the relativistic effect between σ(Te) and σ(Se).

The $\sigma^{so}(Te)_{Rlt\text{-}so}$ values cause upfield shifts of 331 to 889 ppm for the various tellurium species. Figure 5 shows the plot of $\sigma^{so}(Te)_{Rlt\text{-}so}$ versus $\Delta\sigma^{p}(Te)_{Rlt\text{-}so}$. To understand the structural dependence of the plot, the data are analyzed by dividing into four groups, **G1**–**G4**, although tentative. Data of HTe^{-} and $MeTe^{-}$ belong to **G1** (group 1), together with MeTeTeMe. The $\sigma^{so}(Te)_{Rlt\text{-}so}$ values cause large upfield shifts of 824 to 888 ppm with the $\Delta\sigma^{p}(Te)_{Rlt:so}$ range of –109 to –375 ppm. **G2** consists of hydrogen telluride derivatives of the H_nTe* form where * =

Table 1 The σ^{d}(Te), σ^{p}(Te), σ^{d+p}(Te), σ^{so}(Te) and σ^{t}(Te) Values Calculated at the BLYP Level with the QZ4Pae Basis Sets Under the Nonrelativistic (Non) and Spin-orbit ZORA Relativistic (Rlt-so) Conditions for Various Tellurium Species[a–d]

Species	σ^{d}_{Non}	σ^{p}_{Non}	σ^{d+p}_{Non}	σ^{d}_{Rlt-so}	$\Delta\sigma^{d}_{Rlt-so}$	σ^{p}_{Rlt-so}	$\Delta\sigma^{p}_{Rlt-so}$	σ^{d+p}_{Rlt-so}	$\Delta\sigma^{d+p}_{Rlt-so}$	σ^{so}_{Rlt-so}	σ^{t}_{Rlt-so}	$\Delta\sigma^{t}_{Rlt-so}$
H_2Te (C_{2v})	5360.1	-1856.4	3503.6	5302.6	-57.5	-2006.3	-149.8	3296.3	-207.3	743.5	4039.9	536.2
HTe^- ($C_{\infty v}$)	5365.2	-993.7	4371.5	5308.4	-56.8	-1102.6	-108.9	4205.8	-165.7	823.9	5029.7	658.2
H_3Te^+ (C_{3v})	5353.7	-2167.7	3186.1	5296.4	-57.3	-2292.2	-124.5	3004.3	-181.8	639.0	3643.3	457.2
H_4Te (C_{2v})	5356.4	-1756.7	3599.7	5299.2	-57.2	-1872.3	-115.6	3426.9	-172.8	741.6	4168.5	568.8
H_5Te^- (C_{4v})	5350.4	-1983.0	3367.4	5293.9	-56.5	-2036.2	-53.1	3257.7	-109.6	557.2	3814.9	447.6
H_5Te^+ (C_{4v})	5348.2	-2359.8	2988.5	5289.8	-58.5	-2447.1	-87.3	2842.6	-145.8	645.0	3487.6	499.2
H_6Te (O_h)	5342.6	-2169.8	3172.8	5285.1	-57.5	-2231.4	-61.5	3053.8	-119.0	659.0	3712.8	540.0
$MeTe^-$ (C_s)	5366.0	-2252.0	3114.0	5309.3	-56.7	-2436.1	-184.1	2873.2	-240.8	888.5	3761.8	647.8
MeTeH (C_s)	5361.3	-2312.2	3049.0	5304.3	-57.0	-2479.5	-167.3	2824.8	-224.3	741.1	3565.9	516.9
Me_2Te (C_{2v})	5362.5	-2719.1	2643.4	5305.9	-56.6	-2890.6	-171.5	2415.3	-228.1	725.2	3140.5	497.1
EtTeH (C_s)	5360.9	-2392.9	2968.0	5304.2	-56.7	-2568.4	-175.5	2735.8	-232.2	716.4	3452.2	484.2
Et_2Te (C_{2v})	5362.9	-2911.9	2450.9	5306.4	-56.5	-3105.8	-193.8	2200.6	-250.4	686.3	2886.8	435.9
MeTeTeMe (C_2)	5364.1	-2736.1	2628.0	5307.3	-56.7	-3110.7	-374.6	2196.7	-431.3	884.9	3081.6	453.6
Me_3Te^+ (C_3)	5357.0	-2954.6	2402.4	5300.2	-56.8	-3121.3	-166.7	2178.9	-223.5	634.0	2812.8	410.5
Me_4Te (C_{2v})	5357.5	-2399.5	2958.0	5300.6	-56.9	-2549.8	-150.3	2750.8	-207.2	718.2	3469.0	511.0
Me_5Te^- (C_s)	5351.5	-2465.2	2886.4	5294.6	-56.9	-2558.7	-93.6	2735.9	-150.5	560.8	3296.7	410.3
Me_5Te^+ (C_s)	5352.3	-2978.8	2373.5	5293.5	-58.8	-3111.9	-133.1	2181.5	-192.0	626.7	2808.3	434.8
Me_6Te (C_i)	5348.9	-2542.4	2806.5	5287.2	-61.7	-2638.7	-96.3	2648.5	-158.0	649.5	3298.0	491.5
H_2TeF_2 (C_{2v})	5349.6	-3146.3	2203.4	5292.5	-57.2	-3351.6	-205.3	1940.8	-262.5	507.1	2447.9	244.6
H_2TeO (C_s)	5354.2	-3280.6	2073.6	5297.0	-57.2	-3497.8	-217.2	1799.2	-274.4	563.2	2362.4	288.8
H_2TeO_2 (C_{2v})	5354.2	-3433.9	1920.3	5296.3	-57.9	-3656.5	-222.6	1639.8	-280.5	549.0	2188.8	268.5
H_4TeO (C_{2v})	5349.8	-2705.3	2644.5	5291.5	-58.3	-2834.0	-128.7	2457.5	-187.0	598.0	3055.5	411.0
H_2TeF_2O (C_{2v})	5349.0	-3262.8	2086.2	5292.1	-56.9	-3480.2	-217.4	1812.0	-274.2	550.9	2362.8	276.6
Me_2TeF_2 (C_{2v})	5350.7	-3498.9	1851.8	5294.3	-56.4	-3741.6	-242.7	1552.7	-299.1	506.8	2059.5	207.7
$(CF_3)_2TeF_2$ (C_{2v})	5351.9	-3472.5	1879.4	5295.6	-56.2	-3732.1	-259.6	1563.6	-315.8	432.1	1995.7	116.3
Me_2TeCl_2 (C_{2v})	5354.4	-3119.7	2234.7	5298.0	-56.3	-3322.4	-202.7	1975.6	-259.1	572.0	2547.6	312.9
Me_2TeBr_2 (C_{2v})	5356.8	-3034.2	2322.7	5299.6	-57.2	-3251.7	-217.5	2048.0	-274.7	542.0	2590.0	267.4
Me_2TeO (C_s)	5356.3	-3591.0	1765.3	5299.1	-57.2	-3828.0	-237.0	1471.1	-294.2	570.0	2041.1	275.8
Me_2TeO_2 (C_{2v})	5355.9	-3681.1	1674.8	5298.7	-57.2	-3936.7	-255.6	1362.0	-312.9	555.5	1917.4	242.6
Me_2TeF_2O (C_{2v})	5350.4	-3494.5	1855.9	5293.7	-56.7	-3739.8	-245.3	1553.9	-302.0	549.3	2103.1	247.2
F_2TeO (C_s)	5351.5	-4143.6	1207.9	5294.8	-56.7	-4530.0	-386.4	764.7	-443.1	388.1	1152.9	-55.0
Cl_2TeO (C_s)	5353.9	-4335.1	1018.8	5298.2	-55.7	-4735.4	-400.2	562.9	-455.9	438.8	1001.7	-17.1
F_2TeO_2 (C_{2v})	5351.2	-3492.0	1859.2	5293.5	-57.7	-3756.0	-264.1	1537.4	-321.8	508.7	2046.1	186.9
TeF_4 (C_{2v})	5345.9	-3671.4	1674.4	5289.1	-56.8	-3983.2	-311.7	1305.9	-368.5	331.0	1636.9	-37.5
$TeCl_4$ (C_{2v})	5349.1	-4157.4	1191.7	5294.9	-54.3	-4562.3	-404.8	732.6	-459.0	469.5	1202.1	10.5
TeF_5^- (C_{4v})	5340.6	-3426.1	1914.5	5284.7	-55.9	-3709.5	-283.4	1575.2	-339.3	347.2	1922.4	7.9
TeF_5^+ (C_{4v})	5345.6	-3240.8	2104.8	5288.2	-57.4	-3509.7	-268.9	1778.4	-326.4	640.9	2419.4	314.5
$HTeF_5$ (C_{4v})	5342.2	-3128.6	2213.7	5282.4	-59.8	-3385.6	-257.1	1896.8	-316.9	629.9	2526.6	313.0
$MeTeF_5$ (C_s)	5341.4	-3234.9	2106.4	5283.9	-57.5	-3494.5	-259.6	1789.4	-317.0	601.6	2391.0	284.6
TeF_6 (O_h)	5340.1	-3047.1	2293.0	5283.6	-56.5	-3301.1	-254.0	1982.5	-310.5	649.6	2632.1	339.1

[a] Structures optimized at the $MP2_{Non}$ level of Gaussian 03 being employed. [b] σ(Te) (in ppm) are denoted by σ in Table. [c] $\Delta\sigma_{Rlt-so} = \sigma_{Rlt-so} - \sigma_{Non}$. [d] $\Delta\sigma^{t}_{Rlt-so} = \sigma^{t}_{Rlt-so} - \sigma^{d+p}_{Non} = \Delta\sigma^{d+p}_{Rlt-so} + \sigma^{so}_{Rlt-so}$.

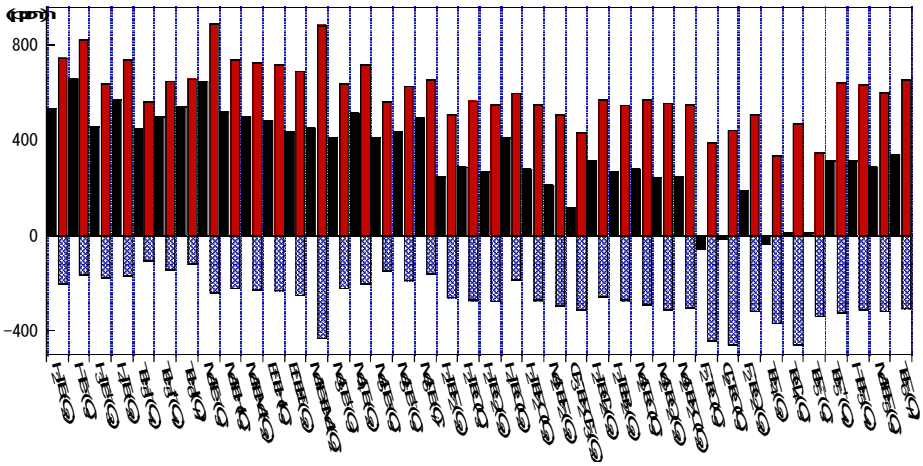

Fig. 1 Relativistic effect on σ(Te) for various tellurium compounds calculated at the BLYP level with QZ4Pae under Non and Rlt-so conditions: ■, ■ and ■ stand for the total term ($\Delta\sigma^{t}(Te)_{Rlt-so} = \Delta\sigma^{d+p}(Te)_{Rlt-so} + \sigma^{so}(Te)_{Rlt-so}$), the scalar term ($\Delta\sigma^{d+p}(Te)_{Rlt-so}$) and the spin-orbit term ($\sigma^{so}(Te)_{Rlt-so}$), respectively. Values are from Table 1, evaluated on the structures optimized at the $MP2_{Non}$ level.

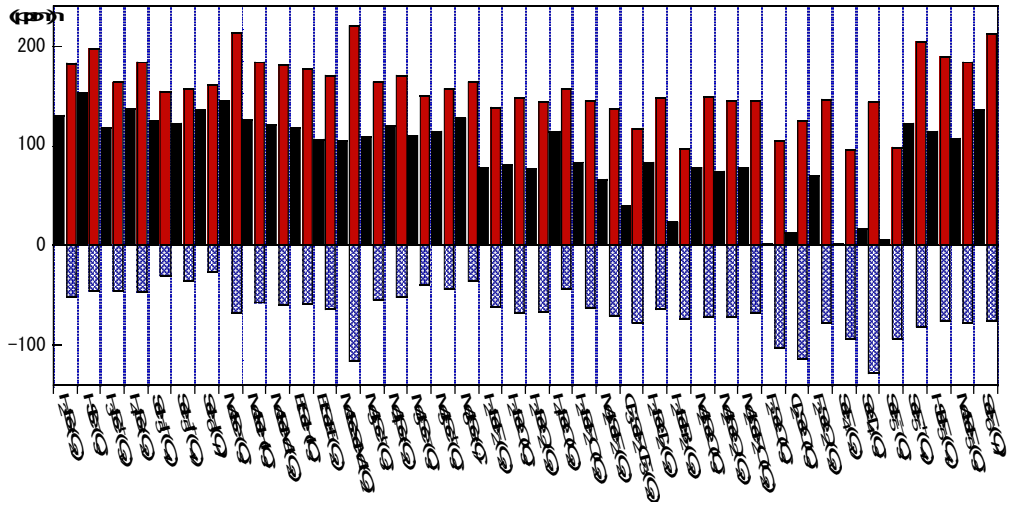

Fig. 2 Relativistic effect on σ(Se) for various selenium compounds calculated at the BLYP level with QZ4Pae under Non and Rlt-so conditions: ■, ■ and ■ stand for the total term ($\Delta\sigma^{t}(Se)_{Rlt\text{-}so} = \Delta\sigma^{d+p}(Se)_{Rlt\text{-}so} + \sigma^{so}(Se)_{Rlt\text{-}so}$), the scalar term ($\Delta\sigma^{d+p}(Se)_{Rlt\text{-}so}$) and the spin-orbit term ($\sigma^{so}(Se)_{Rlt\text{-}so}$), respectively. Values are from Table S2, evaluated on the structures optimized at the $MP2_{Non}$ level.

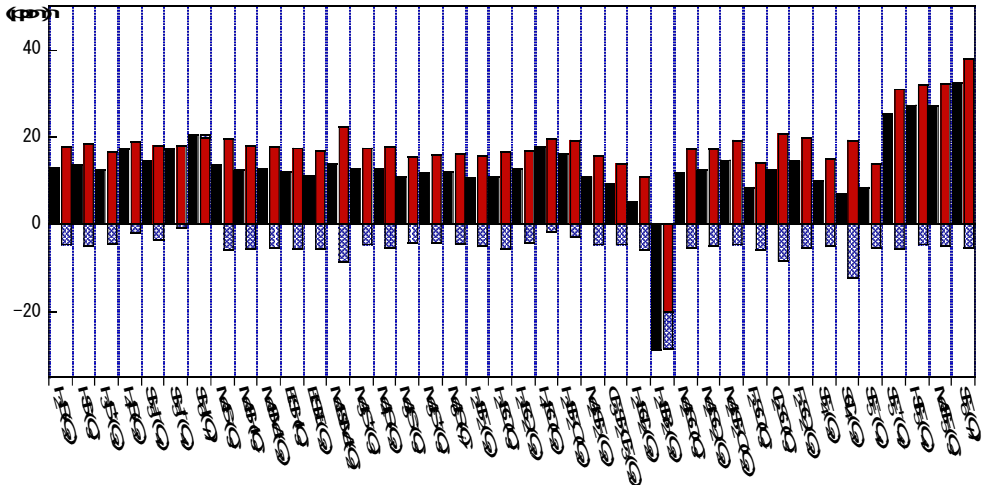

Fig. 3 Relativistic effect on σ(S) for various sulfur compounds calculated at the BLYP level with QZ4Pae under Non and Rlt-so conditions: ■, ■ and ■ stand for the total term ($\Delta\sigma^{t}(S)_{Rlt\text{-}so} = \Delta\sigma^{d+p}(S)_{Rlt\text{-}so} + \sigma^{so}(S)_{Rlt\text{-}so}$), the scalar term ($\Delta\sigma^{d+p}(S)_{Rlt\text{-}so}$) and the spin-orbit term ($\sigma^{so}(S)_{Rlt\text{-}so}$), respectively. Values are from Table S3, evaluated on the structures optimized at the $MP2_{Non}$ level.

null, + and –, which correspond to neutral, cationic and anionic species, respectively, with n = 1 – 6. The alkyl derivatives of H_nTe* also belong to **G2**. The range of $\sigma^{so}(Te)_{Rlt\text{-}so}$ in **G2** is 557 to 744 ppm with $-194 < \Delta\sigma^{p}(Te)_{Rlt\text{-}so} < -53$ ppm. **G3** is formed with the data for H_2TeX_2, H_2TeO, H_2TeO_2 and the alkyl derivatives. Data for TeF_5^+, $RTeF_5^-$, $RTeF_5$ and TeF_6 are contained in **G3** for convenience of explanation. The $\sigma^{so}(Te)_{Rlt\text{-}so}$ values in **G3** cover the range of 432 to 650 ppm with $-269 < \Delta\sigma^{p}(Te)_{Rlt\text{-}so} < -203$ ppm, together with $\Delta\sigma^{p}(Te)_{Rlt\text{-}so} = -129$ ppm for H_4TeO. The $\sigma^{so}(Te)_{Rlt\text{-}so}$ values for $TeCl_4$, Cl_2TeO, F_2TeO, TeF_4 and TeF_5^- are in **G4**. The plot shows convex downward. The ranges of $\sigma^{so}(Te)_{Rlt\text{-}so}$ and $\Delta\sigma^{p}(Te)_{Rlt\text{-}so}$ are from 470 to 331 ppm and from –405 to –284 ppm, respectively. The results are very similar to those for $\sigma^{so}(Se)_{Rlt\text{-}so}$, which anticipates us the linear relation again in the relativistic effect between σ(Te) and σ(Se).[14]

Figure 6 shows the plots of $\sigma^{d+p}(Te)_{Rlt\text{-}so}$ and $\sigma^{t}(Te)_{Rlt\text{-}so}$ versus $\sigma^{d+p}(Te)_{Non}$. The correlations are collected in entries 2 and 3 in Table 2, of which a values are 1.10 and 1.24, respectively. The a value of 1.10 in entry 2 must be the reflection from the relativistic effect on $\sigma^{d+p}(Te)_{Rlt\text{-}so}$ more downfield shifts for higher coordinated species by about 10% as a whole, especially for the effect on $\sigma^{p}(Te)_{Rlt\text{-}so}$ (see entry 1 in Table 2). Similarly, a = 1.24 in entry 3 can be explained by more upfield shifts of $\sigma^{so}(Te)_{Rlt\text{-}so}$ for the lower coordinated species by about 14% as a whole, in addition to more downfield shifts in $\sigma^{d+p}(Te)_{Rlt\text{-}so}$ (or $\sigma^{p}(Te)_{Rlt\text{-}so}$) for higher coordinated species, as a whole. The correlation of $\sigma^{t}(Te)_{Rlt\text{-}so}$ versus $\sigma^{d+p}(Te)_{Rlt\text{-}so}$ is given in entry 4 of Table 2 of which a value is 1.12, although the plot is not shown. The a value of 1.24 in entry 3 seems to be explained by the product between a = 1.10 (entry 2) and a = 1.12 (entry 4) (1.10 × 1.12 = 1.23).

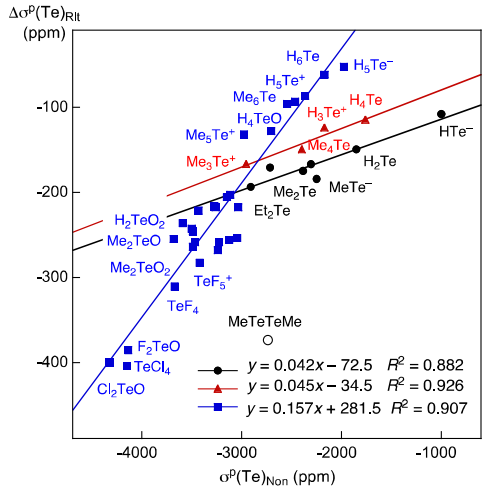

Fig. 4 Plot of $\Delta\sigma^{p}(Te)_{Rlt\text{-}so}$ versus $\sigma^{p}(Te)_{Non}$: ●, ▲ and ■ stand for mono- and di-coordinated species, R_3Te^+ and R_4Te species where R = H and Me, and other species in Table 1, respectively, with ○ for MeTeTeMe. The plot is analyzed as three linear correlations, which are given in the Figure.

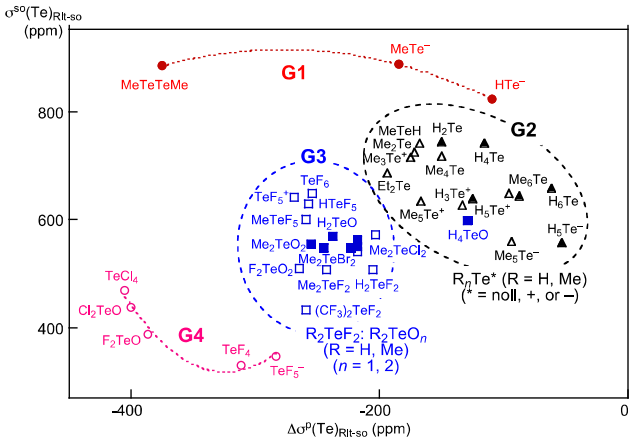

Fig. 5 Plots of $\sigma^{so}(Te)_{Rlt\text{-}so}$ versus $\Delta\sigma^{p}(Te)_{Rlt\text{-}so}$. $\sigma^{so}(Te)_{Rlt\text{-}so}$ are tentatively divided into four groups: **G1** in red, **G2** in black, **G3** in blue and **G4** in pink.

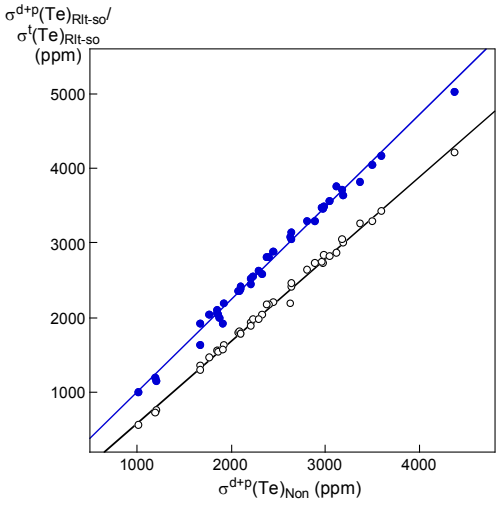

Fig. 6 Plots of $\sigma^{d+p}(Te)_{Rlt\text{-}so}$ (○) and $\sigma^{t}(Te)_{Rlt\text{-}so}$ (●) versus $\sigma^{d+p}(Te)_{Non}$.

After elucidation of the relativistic effect on σ(Te), next extension is to clarify the trends in the relativistic effect on σ(S), σ(Se) and σ(Te), as a series of the group 16 element.

Trends in the Relativistic Effect on σ(Te), σ(Se) and σ(S)

The relativistic effect on each of σ(Te), σ(Se) and σ(S) is summarized in Table S7 of the Supporting Information. Table S7 also contains the correlations given in Table 2. The trends in the relativistic effect on σ(Te), σ(Se) and σ(S) will be discussed taking the effect on σ(Se) as the standard.

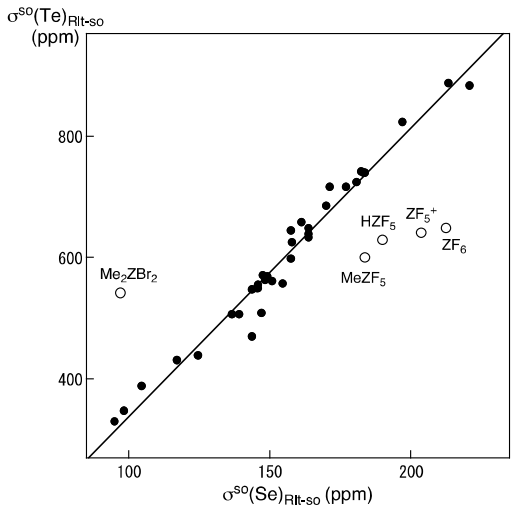

Fig. 7 Plot of $\sigma^{so}(Te)_{Rlt\text{-}so}$ versus $\sigma^{so}(Se)_{Rlt\text{-}so}$. Data of Me_2ZBr_2, $MeZF_5$, HZF_5, ZF_5^+ and ZF_6 (Z = Te versus Se) deviate from the correlation.

Table 2 Correlations in σ(Z) or Δσ(Z) (Z = Te, Se and S) for Various Species Containing Z, Evaluated at the BLYP Level with the QZ4Pae Basis Sets, Under Non and Rlt-so Conditions[a]

Entry	Correlation	*a*	*b*	R^2	*n*
1	$\sigma^{p}(Te)_{Rlt\text{-}so}$ *vs.* $\sigma^{p}(Te)_{Non}$	1.103	92.5	0.995	40
1'	$\sigma^{p}(Te)_{Rlt\text{-}so}$ *vs.* $\sigma^{p}(Te)_{Non}$	1.105	103.2	0.997	39[b]
2	$\sigma^{d+p}(Te)_{Rlt\text{-}so}$ *vs.* $\sigma^{d+p}(Te)_{Non}$	1.102	–510.9	0.996	40
3	$\sigma^{t}(Te)_{Rlt\text{-}so}$ *vs.* $\sigma^{d+p}(Te)_{Non}$	1.236	–232.6	0.992	40
4	$\sigma^{t}(Te)_{Rlt\text{-}so}$ *vs.* $\sigma^{d+p}(Te)_{Rlt\text{-}so}$	1.119	348.3	0.990	40
5	$\sigma^{d+p}(Te)_{Rlt\text{-}so}$ *vs.* $\sigma^{d+p}(Se)_{Rlt\text{-}so}$	1.331	568.0	0.963	40
6	$\sigma^{t}(Te)_{Rlt\text{-}so}$ *vs.* $\sigma^{t}(Se)_{Rlt\text{-}so}$	1.460	787.6	0.969	40
7	$\Delta\sigma^{d+p}(Te)_{Rlt\text{-}so}$ *vs.* $\Delta\sigma^{d+p}(Se)_{Rlt\text{-}so}$	3.783	–16.3	0.963	40
8	$\sigma^{so}(Te)_{Rlt\text{-}so}$ *vs.* $\sigma^{so}(Se)_{Rlt\text{-}so}$	4.780	–140.4	0.969	35[c]
9	$\Delta\sigma^{t}(Te)_{Rlt\text{-}so}$ *vs.* $\Delta\sigma^{t}(Se)_{Rlt\text{-}so}$	4.576	–74.2	0.979	35[c]

[a] The constants (*a*, *b*, R^2) are the correlation constant, the *y*-intercept and the square of correlation coefficient, respectively, in $y = ax + b$. [b] Neglecting the data of MeTeTeMe. [c] Neglecting the data of Me_2ZBr_2, $MeZF_5$, HZF_5, ZF_5^+ and ZF_6.

Correlations of $\sigma^{d+p}(Te)_{Rlt\text{-}so}$ versus $\sigma^{d+p}(Se)_{Rlt\text{-}so}$ and $\sigma^{t}(Te)_{Rlt\text{-}so}$ versus $\sigma^{t}(Se)_{Rlt\text{-}so}$ are given in entries 5 and 6 of Table 2, respectively, of which *a* values are 1.33 and 1.46, respectively. The increase in *a* of 1.33 to 1.46 must be the result of the larger relativistic effect on $\sigma^{so}(Te)_{Rlt\text{-}so}$ relative to the case of $\sigma^{so}(Se)_{Rlt\text{-}so}$. The correlation of $\Delta\sigma^{d+p}(Te)_{Rlt\text{-}so}$ versus $\Delta\sigma^{d+p}(Se)_{Rlt\text{-}so}$ is given in entry 7 of Table 2 (*a* = 3.78). How is the correlation of $\sigma^{so}(Te)_{Rlt\text{-}so}$ versus $\sigma^{so}(Se)_{Rlt\text{-}so}$? Figure 7 shows the plot of $\sigma^{so}(Te)_{Rlt\text{-}so}$ versus $\sigma^{so}(Se)_{Rlt\text{-}so}$. The plot gives

good correlation, except for the data of Me_2ZBr_2, $MeZF_5$, HZF_5, ZF_5^+ and ZF_6 (Z = Te versus Se). The correlation of the plot is given in entry 8 of Table 2 (a = 4.78), although the deviated data are omitted in the correlation. The correlation for $\Delta\sigma^t(Te)_{Rlt\text{-}so}$ versus $\Delta\sigma^t(Se)_{Rlt\text{-}so}$ is shown in entry 9 of Table 2. The a value of 4.58 is close to 5, showing the relativistic effect on σ^t(Te) being about five times larger than that on σ^t(Se), again. The results support the conclusion that the magnitude of the relativistic effect becomes smaller in the order of σ(Te) >> σ(Se) >> σ(S). The ratios are approximately 25 : 5 : 1, where the relativistic effect on σ(S) is summarized in Table S7, although not discussed in detail here.

After clarification of the relativistic effect on σ(S), σ(Se) and σ(Te) as a series of group 16 elements, next extension is to examine the applicability of $\sigma^t(Te)_r$ to $\delta(Te)_{obsd}$.

Applicability of σ^t(Te: M)$_r$ to Analyze δ(Te: M)$_{obsd}$

To confirm the reliability of the calculation method, it is inevitable to demonstrate the applicability of σ^t(Te: **M**)$_r$ to analyze δ(Te: **M**)$_{obsd}$. σ^t(Te: **M**)$_r$ are defined as [–(σ^t(Te: **M**) – σ^t(Te: Me_2Te))], where σ^t(Te: **M**) stand for σ^t calculated for Te in a molecule **M**. The sign of σ^t(Te: **M**)$_r$ is set up equal to that of δ(Te: **M**)$_{obsd}$ in the definition, which is employed in this paper. The δ(Te: **M**)$_{obsd}$ values are reported for **M** of several compounds if limited to those in Table 1. Therefore, σ(Te) of 46 tellurium species (**1**–**46**), almost other than the 40 species, are calculated to accomplish the purpose. Chart 1 draws some structures. The conformational effect must affect much on σ^t(Te), therefore, they must be carefully examined in the prediction of $\sigma^t(Te)_r$. Figure 8 draws some conformers for **M** of MeTeEt (**8**: **8a** and **8b**), EtTeEt (**10**: **10a**, **10b** and **10c**), EtTeTeEt (**13**: **13a**, **13b** and **13c**) and PhTeTePh (**18**: **18a** and **18b**). Conformers of **10a**, **10b** and **10c** correspond to (*trans*, *trans*) of the C_2 symmetry, (*trans*, *gauche*) of C_1 and (*gauche*, *gauche*) of C_2 around the two CTeCC sequences, respectively, in **10**. While the Te-Te bond is nearly on both phenyl planes in **18a**, it is almost perpendicular to the planes in **18b**.

While the σ^{d+p}(Te: **M**)$_{Rlt\text{-}so:r}$ and $\sigma^{\square}$(Te: **M**)$_{Rlt\text{-}so:r}$ values are evaluated at the $OPBE_{Rlt\text{-}so}$//$OPBE_{Rlt\text{-}so}$ method, σ^{d+p}(Te: **M**)$_{Non:r}$ are at the $OPBE_{Non}$//$OPBE_{Rlt\text{-}so}$ method. The $\sigma^{\square}$(Te: **M**)$_{Rlt\text{-}so:r}$ values are similarly evaluated with $BLYP_{Rlt\text{-}so}$//$OPBE_{Rlt\text{-}so}$ and $BLYP_{Rlt\text{-}so}$//$MP2_{Non}$. Table 3 collects the results for the compounds with the compound numbers. Table 3 also contains σ(Te: **M**)$_r$ for some conformers in **M** of **8**, **10**, **13** and **18**. Simple averaged values of $\sigma^{\square}$(Te: **M**)$_{Rlt\text{-}so:r}$ over the conformers are employed for discussion, in spite of the different energies for the conformers, since the energy differences are not so large and the population of each conformer may change depending on the conditions of measurements, such as the solvent.

The systematic behavior is predicted for σ^t(Te: **10**)$_{Rlt\text{-}so:r}$. The value shifts more down field by about 40 ppm for each process in the change from **10a** to **10b** then to **10c**, if calculated with $OPBE_{Rlt\text{-}so}$//$OPBE_{Rlt\text{-}so}$. Similar trend is observed for the values evaluated with $BLYP_{Rlt\text{-}so}$//$OPBE_{Rlt\text{-}so}$ and $BLYP_{Rlt\text{-}so}$//$MP2_{Non}$, although the shift values are not the same. The σ^t(Te: **8**)$_{Rlt\text{-}so:r}$ value also goes more down field by 60–70 ppm for the process from **8a** to **8b**, calculated with the three method.

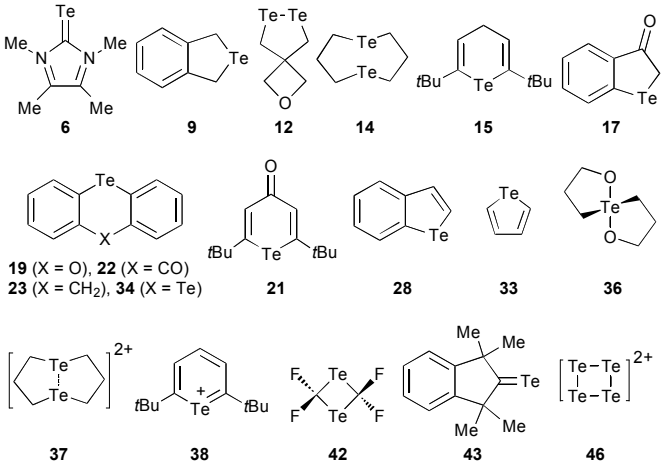

Chart 1. Some structures of tellurium compounds, examined.

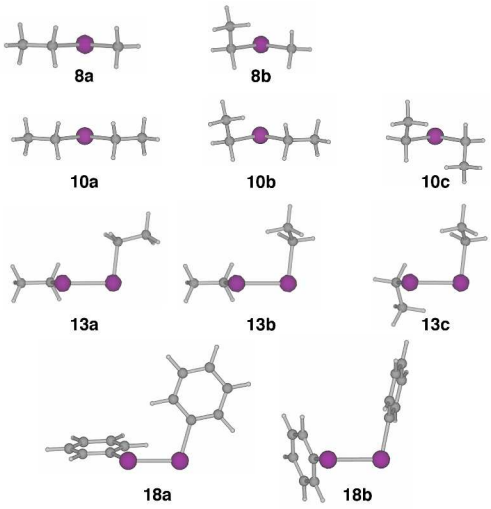

Fig. 8 Conformers of **8**, **10**, **13** and **18**.

The $\sigma^{\square}$(Te: **13**)$_{Rlt\text{-}so:r}$ value shifts more downfield when **13a** (118.2 ppm) goes **13b** (148.5 ppm) then to **13c** (181.0 ppm), similarly to the case of EtTeEt (**10**), if calculated with $BLYP_{Rlt\text{-}so}$//$MP2_{Non}$. However, the value does more upfield, if calculated with $OPBE_{Rlt\text{-}so}$//$OPBE_{Rlt\text{-}so}$, which is just the opposite trend to those with $BLYP_{Rlt\text{-}so}$//$MP2_{Non}$. Much attention should be paid to the torsional angles of ϕ(CTeTeC) in **13**, which decease in the order of **13a** (83.6º), **13b** (72.6º) and **13c** (69.3º), if optimized with $OPBE_{Rlt\text{-}so}$. The optimized structures of **13a**, **13b** and **13c** with $OPBE_{Rlt\text{-}so}$ must be responsible for the opposite trend. The inverse trend in $\sigma^{\square}$(Te: **13**)$_{Rlt\text{-}so:r}$ seems improved (by roughly half), if employed the structures optimized with $OPBE_{Rlt\text{-}so}$, of which ϕ(CTeTeC) being fixed at 90.0º. The structural parameters and $\sigma^{\square}$(Te: **M**)$_{Rlt\text{-}so:r}$ calculated under some conditions are summarized in Table 4.

Table 3 The σ^{d+p}(Te: **M**)$_{Non:r}$, σ^{d+p}(Te: **M**)$_{Rlt\text{-}so:r}$ and/or $\sigma^{□}$(Te: **M**)$_{Rlt\text{-}so:r}$ Values Calculated at the BLYP and OPBE Levels Under the Nonrelativistic (Non) and Spin-orbit ZORA Relativistic (Rlt-so) Conditions with the QZ4Pae Basis Sets for Various Tellurium Species,[a] Together with the δ(Te)$_{obsd}$ Values[b]

Species (No) Basis Set: Evaluation of $\sigma^{□}$(Te: **M**) Basis Set: Structural Optimization	σ^{d+p}(Te: **M**)$_{Non:r}$ OPBE$_{Rlt\text{-}so}$ OPBE$_{Non}$	σ^{d+p}(Te: **M**)$_{Rlt\text{-}so:r}$ OPBE$_{Rlt\text{-}so}$ OPBE$_{Rlt\text{-}so}$	$\sigma^{□}$(Te: **M**)$_{Rlt\text{-}so:r}$ OPBE$_{Rlt\text{-}so}$ OPBE$_{Rlt\text{-}so}$	$\sigma^{□}$(Te: **M**)$_{Rlt\text{-}so:r}$ BLYP$_{Rlt\text{-}so}$ OPBE$_{Rlt\text{-}so}$	$\sigma^{□}$(Te: **M**)$_{Rlt\text{-}so:r}$ BLYP$_{Rlt\text{-}so}$ MP2$_{Non}$	δ(Te: **M**)$_{obsd}$	Solvent/Comment
$TeMe_2$ (C_{2v}: **1**)	0.0	0.0	0.0	0.0	0.0	0.0	neart/refs. 28-30
$TeP(iPr)_3$ (C_1: **2**)	-1145.0	-1119.3	-1201.7	-1168.4	-1360.7	-1000.3	ref. 31
$Te(SiMe_3)_2$ (C_{2v}: **3**)	-1012.0	-1041.8	-1053.0	-1078.0	-1106.5	-842	ref. 32
TeH_2 (C_{2v}: **4**)	-778.0	-813.1	-820.9	-927.0	-899.4	-621	refs. 33,35
$TePMe_3$ (C_1: **5**)	-900.7	-841.8	-916.2	-883.6	-881.4	-513.4	ref. 31
cyclo-$(CMeNMe)_2C{=}Te$ (C_{2v}: **6**)	-271.1	-197.6	-257.1	-296.5	-301.6	-168	ref. 35
$TeMe_4$ (C_{2v}: **7**)	-132.0	-166.0	-116.0	-188.2	-145.2	-67.0	C_6D_6/ref. 36
MeTeEt (av: **8**)	121.0	140.8	149.1	164.9	156.2	165	$CDCl_3$/ref. 37
MeTeEt (C_s: **8a**) (as 0.0)	89.3	100.0	117.1	129.0	120.0		
MeTeEt ($C_{1\text{-}g}$: **8b**) (–2.9)	152.7	181.6	181.0	200.8	192.3		
cyclo-$C_6H_4(CH_2)_2Te$ (C_2: **9**)	211.6	242.1	241.7	237.1	123.6	269	$(CD_3)_2NCHO$/refs. 29,38
EtTeEt (av: **10**)	250.2	290.1	306.7	337.6	309.1	356	$CDCl_3$/ref. 37
EtTeEt (C_{2v}: **10a**) (as 0.0)	207.4	232.2	265.4	291.4	253.6		
EtTeEt ($C_{1\text{-}g}$: **10b**) (–2.7)	250.5	291.5	308.6	341.8	323.8		
EtTeEt ($C_{2\text{-}gg}$: **10c**) (–7.1)	292.7	346.6	346.2	379.7	349.7		
MeTeTeMe (C_2: **11**)	-36.2	154.6	5.1	40.9	58.9	49	$CDCl_3$/ref. 34
spiro-$Te_2C_5H_8O$ (C_1: **12**)	37.1	177.4	88.3	85.1	51.9	57.1	ref. 39
EtTeTeEt (av: **13**)	28.9	238.3	101.2	180.2	149.2	166	CD_2Cl_2/ref. 40
EtTeTeEt (C_2: **13a**) (as 0.0)	84.9	293.8	160.2	180.2	118.2		
EtTeTeEt ($C_{1\text{-}g}$: **13b**) (–4.4)	11.8	229.4	96.9		148.5		
EtTeTeEt ($C_{2\text{-}gg}$: **13c**) (–8.6)	-10.0	191.8	46.4		181.0		
cyclo-$Te(CH_2CH_2CH_2)_2Te$ (C_{2v}: **14**)	73.6	115.6	110.2	149.9	354.1	164	ref. 41
cyclo-$Te(C(t\text{Bu})CH)_2CH_2$ (C_s: **15**)	140.8	192.7	225.5	173.2	162.1	257	ref. 42
PhTeMe (C_s: **16**)	314.7	369.6	383.4	404.7	404.5	329	$CDCl_3$/ref. 37
cyclo-$C_6H_4TeCH_2CO$ (C_s: **17**)	160.9	184.8	219.6	172.8	221.4	383	$CDCl_3$/ref. 43
PhTeTePh (av: **18**)	719.3	619.4	360.0	407.4	447.4	420	$CDCl_3$/ref. 44
PhTeTePh (C_2: **18a**) (as 0.0)	1326.3	904.4	514.1	595.3	629.9		
PhTeTePh (C_2: **18b**) (–2.1)	112.3	334.4	205.9	219.4	264.9		
cyclo-$Te(C_6H_4)_2O$ (C_s: **19**)	247.4	281.2	339.3	305.5	355.7	424	$CDCl_3$/ref. 43
Me_3Te^+ (C_3: **20**)	308.5	302.7	392.7	307.4	327.7	408[c]	ref. 45
cyclo-$Te(C(t\text{Bu})CH)_2CO$ (C_{2v}: **21**)	239.5	295.0	335.6	273.1	261.3	445	ref. 42
cyclo-$Te(C_6H_4)_2CO$ (C_s: **22**)	222.0	248.1	325.3	281.3	316.6	468	$CDCl_3$/ref. 43
cyclo-$Te(C_6H_4)_2CH_2$ (C_s: **23**)	345.0	398.5	455.5	417.2	447.7	512	$CDCl_3$/ref. 43
TeF_6 (O_h: **24**)	458.1	532.6	611.7	445.9	508.4	545	neat/refs. 28,29
$PhTeCH{=}CH_2$ (C_1: **25**)	475.5	547.9	593.7	588.7	590.1	615	ref. 46
PhTePh (C_2: **26**)	573.3	667.9	703.7	713.2	662.1	688	$CDCl_3$/refs. 34,44
$CF_3TeTeCF_3$ (C_2: **27**)	497.0	769.5	663.5	786.5	664.8	686	$CDCl_3$/ref. 47
cyclo-$C_6H_4TeCH{=}CH$ (C_1: **28**)	499.9	574.9	628.9	561.3	590.2	727	$CDCl_3$/ref. 48
Me_2TeCl_2 (C_{2v}: **29**)	495.0	526.4	682.5	639.5	592.9	734	ref. 49
Me_2TeBr_2 (C_{2v}: **30**)	402.1	449.0	633.3	610.7	550.5	649	ref. 49
$PhTeCl_2Me$ (C_1: **31**)	561.3	609.8	774.9	735.5	648.8	809.7[d]	$CDCl_3$/this work
$PhTeBr_2Me$ (C_1: **32**)	480.6	548.1	729.5	709.5	603.0	744.6[d]	$CDCl_3$/this work
cyclo-$Te(CH)_4$ (C_{2v}: **33**)	523.0	613.4	671.3	591.6	623.0	782	$(CD_3)_2CO$/ref. 50
cyclo-$Te(C_6H_4)_2Te$ (C_{2v}: **34**)	771.7	876.0	978.1	955.5	919.7	888	ref. 51
$Te(t\text{Bu})_2$ (C_2: **35**)	912.7	1060.0	1091.7	1157.4	831.8	992	toluene-d_8/ref. 52
bicyclo-$Te(CH_2CH_2CH_2O)_2$ (C_2: **36**)	905.1	1010.8	1194.4	1118.7	1027.6	1096	ref. 53
cyclo-$[Te(CH_2CH_2CH_2)Te]^{2+}$ (C_{2v}: **37**)	998.1	1215.9	1271.6	1263.6	1517.6	1304[e]	ref. 41
cyclo-$Te^+(C(t\text{Bu})CH)_2CH$ (C_{2v}: **38**)	1088.6	1237.1	1351.2	1271.6	1220.2	1304[f]	ref. 42
CF_3TeCF_3 (C_{2v}: **39**)	1102.5	1258.7	1342.7	1501.4	1279.8	1368	CD_3CN/ref. 54
$CF_3TeF_2CF_3$ (C_{2v}: **40**)	948.1	1046.0	1346.7	1268.9	1144.8	1187	CD_3CN/refs. 42,53,55
CF_3TeCF_2Cl (C_s: **41**)	1251.5	1426.2	1528.6	1680.6	1466.4	1566	CD_3CN/ref. 54
cyclo-$F_2CTe_2CF_2$ (C_2: **42**)	2122.6	2316.0	2369.2	2530.6	2379.3	2321.7	ref. 56
cyclo-$C_6H_4(CMe_2)_2C{=}Te$ (C_2: **43**)	2797.3	2930.1	2893.6	2964.5	2905.9	2858	$CDCl_3$/ref. 55
$TeCl_6^{2-}$ (O_h: **44**)	1202.4	1441.9	1717.2	1778.7	1813.7	1531	ref. 29,57
$TeBr_6^{2-}$ (O_h: **45**)	1225.8	1581.9	1888.0	2008.1	1930.8	1348	ref. 29
cyclo-Te_4^{2+} (C_{2v}: **46**)	2092.8	2414.4	2542.8	2681.6	2911.4	2665	ref. 58

[a] σ^{d+p}(Te: **M**)$_r$ = –(σ^{d+p}(Te: **M**) – σ^{d+p}(Te: Me_2Te)) and σ^{t}(Te: **M**)$_r$ = –(σ^{t}(Te: **M**) – σ^{t}(Te: Me_2Te)) in ppm. [b] See also Refs. 26 and 27. [c] OTf^- is counteranio. [d] This work. [e] BF_4^-/PF_6^- is counteranio. [f] PF_6^- is counteranio.

Table 4 Structural Parameters of EtTeTeEt (**13**), Optimized under $MP2_{Non}$ and $OPBE_{Rlt\text{-}so}$, Together with $\sigma^{\square}(Te)_{Rlt\text{-}so:r}$ Evaluated at $OPBE_{Rlt\text{-}so}$

Compd	*r*(Te, Te) (Å)	*r*(Te, C) (Å)	∠(CTeTeC) (º)	$\sigma^{\square}(Te)_{Rlt\text{-}so:r}$ (ppm)
Optimized with $MP2_{Non}$				
13a (C_2)	2.6685	2.1450	-87.48	72.9
13b (C_1)	2.6694	2.1443	-87.82	98.3
13c (C_2)	2.6702	2.1444	-88.26	123.6
Optimized with $OPBE_{Rlt\text{-}so}$				
13a (C_2)	2.6910	2.1839	-83.63	160.2 (204.1[a])
13b (C_1)	2.6913	2.1813	-72.62	96.9 (189.8[a])
13c (C_2)	2.6907	2.1818	-69.30	46.4 (145.3[a])

[a] ∠(CTeTeC) being fixed at 90.0º.

Torsional angles ∠($C_iTeTeC_{i'}$) of 89.1º and 84.8º are predicted for **18a** and **18b**, respectively, when optimized with $OPBE_{Rlt\text{-}so}$. However, ∠($C_iTeTeC_{i'}$) = 76.8º is predicted for **18a** and much smaller value of 43.1º is for **18b** with $MP2_{Non}$, maybe due to the overestimation of the π-π interaction between the phenyl groups in **18**. The partially optimized structure of **18b** with ∠($C_iTeTeC_{i'}$) fixed at 90.0º is employed for the calculation of $\sigma^{\square}(Te: \mathbf{18})_{Rlt\text{-}so:r}$, instead of the fully optimized **18**. The $\sigma^{t}(Te: \mathbf{18})_{Rlt\text{-}so:r}$ values of 514 and 206 ppm are predicted for **18a** and **18b**, respectively, with $OPBE_{Rlt\text{-}so}//OPBE_{Rlt\text{-}so}$. Table 3 lists $\sigma^{\square}(Te: \mathbf{18})_{Rlt\text{-}so:r}$, thus obtained. The simple average value of 360 ppm explain better $\delta(Te: \mathbf{18})_{obsd}$ of 420 ppm than that of each conformer for **18**. Namely, $\delta(Te)_{obsd}$ can be better explained by assuming the equilibrium between conformers, such as **18a** and **18b**, as expected. The populations would be almost equal or slightly excess for **18b**, judging from the energy difference between the two isomers: **18b** is predicted to be more stable than **18a** by 2 kJ mol^{-1}. The simple averaged values of $\sigma^{t}(Te)_{Rlt\text{-}so:r}$ between **18a** and **18b** seem to explain $\delta(Te: \mathbf{18})_{obsd}$ well, if calculated with $BLYP_{Rlt\text{-}so}//OPBE_{Rlt\text{-}so}$ and $BLYP_{Rlt\text{-}so}//MP2_{Non}$.

Such equilibrium in solutions would often be observed in tellurium species between some structures, other than **18**, which must affect on $\delta(Te)_{obsd}$. Four coordinated tellurium species are the typical example of the cases. The weighed averaged values for the structures in the equilibrium are expected to explain $\delta(Te)_{obsd}$. The effect of the equilibrium on $\sigma^{\square}(Te)_{Rlt\text{-}so:r}$ is discussed in the Supporting Information, exemplified by TeF_4 and $TeMe_4$ (**7**) evaluated with $OPBE_{Rlt\text{-}so}//MP2_{Non}$ and $OPBE_{Rlt\text{-}so}//OPBE_{Rlt\text{-}so}$.[59]

It is instructive to define the differences between the calculated and observed values, $\Delta\sigma\delta(Te: \mathbf{M})_{Rlt\text{-}so:r}$ [= $\sigma^{t}(Te: \mathbf{M})_{Rlt\text{-}so:r} - \delta(Te: \mathbf{M})_{obsd}$]. The applicability of the calculation methods employed here will be examined through discussion of $\Delta\sigma\delta(Te: \mathbf{M})_{Rlt\text{-}so:r}$. Figure 9 shows the plot of $\Delta\sigma\delta(Te: \mathbf{M})_{Rlt\text{-}so:r}$, derived from data in Table 3. The plot is explained separately by three categories: Category 1 (C(**1**)) contains $TeP(iPr)_3$ (**2**), $Te(SiMe_3)_2$ (**3**), TeH_2 (**4**) and $TePMe_3$ (**5**), of which $\delta(Te: \mathbf{M})_{obsd}$ and $\sigma^{\square}(Te: \mathbf{M})_{Rlt\text{-}so:r}$ appear very high field, while C(**3**) consists of the characteristic di-anionic and di-cationic species of $TeCl_6^{2-}$ (**44**), $TeBr_6^{2-}$ (**45**) and *cyclo*-Te_4^{2+} (**46**). C(**2**) forms with all compounds in Table 3 other than C(**1**) and C(**3**) (**1** and **6**–**43**), which are rather usual Te species.

As shown in Figure 9, magnitudes of $\Delta\sigma\delta(Te: \mathbf{M})_{Rlt\text{-}so:r}$ change depending on the calculation method. The magnitudes seem larger in the order of $OPBE_{Rlt\text{-}so}//OPBE_{Rlt\text{-}so} < BLYP_{Rlt\text{-}so}//OPBE_{Rlt\text{-}so} \leq BLYP_{Rlt\text{-}so}//MP2_{Non}$. This expectation is supported by the average values and the standard deviations for $\Delta\sigma\delta(Te)_{Rlt\text{-}so:r}$ ($\bar{x}$/ppm: σ□□□□). The calculated values for C(**2**) with the three methods are (-19.8: 67.8), (-24.4: 100.6) and (-53.2: 90.4), respectively. $\sigma^{t}(Te: \mathbf{M})_{Rlt\text{-}so:r}$ evaluated with $OPBE_{Rlt\text{-}so}//OPBE_{Rlt\text{-}so}$ will be discussed, next.

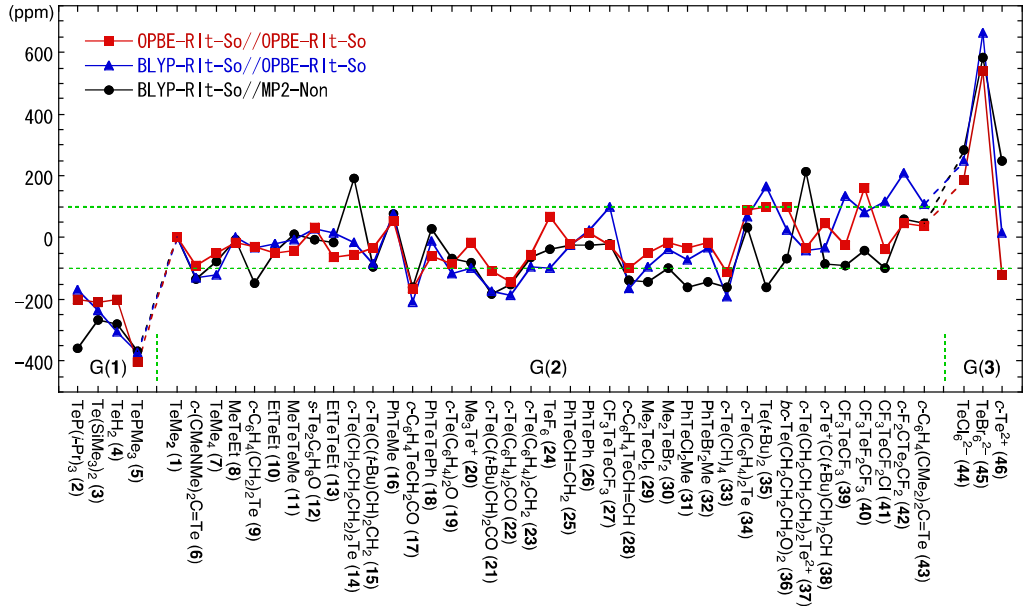

Fig. 9 Plot of $\Delta\sigma\delta(Te: \mathbf{M})_{Rlt\text{-}so:r}$, evaluated with $OPBE_{Rlt\text{-}so}//OPBE_{Rlt\text{-}so}$, $BLYP_{Rlt\text{-}so}//OPBE_{Rlt\text{-}so}$ and $BLYP_{Rlt\text{-}so}//MP2_{Non}$.

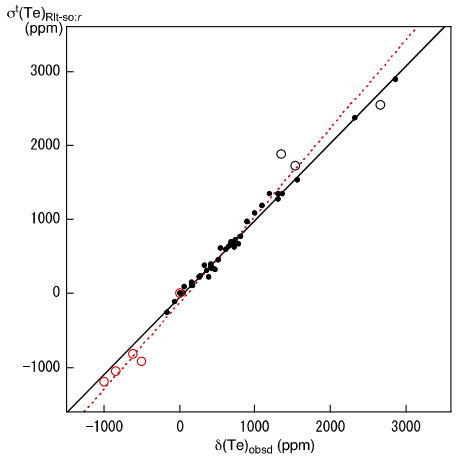

Fig. 10 Plots of σ^t(Te: **M**)$_{Rlt\text{-}so:r}$, evaluated with OPBE$_{Rlt\text{-}so}$//OPBE$_{Rlt\text{-}so}$, versus δ(Te: **M**)$_{obsd}$: Data for **C(1)**, **C(2)** and **C(3)** are shown by ○, ● and ○, respectively.

Table 5 Correlations in the Plots of σ^t(Te: **M**)$_{Rlt\text{-}so:r}$, σ^{d+p}(Te: **M**)$_{Rlt\text{-}so:r}$ and σ^{d+p}(Te: **M**)$_{Non:r}$ versus δ(Te: **M**)$_{obsd}$ for Various Tellurium Species, Evaluated with OPBE$_{Rlt\text{-}so}$//OPBE$_{Rlt\text{-}so}$, BLYP$_{Rlt\text{-}so}$//OPBE$_{Rlt\text{-}so}$, BLYP$_{Rlt\text{-}so}$//MP2$_{Non}$ and the Related Methods with the QZ4Pae Basis Sets[a,b]

Entry	*a*	*b*	R^2	*n*	Applied to	Method
σ^t(Te: **M**)$_{Rlt\text{-}so:r}$ versus δ(Te: **M**)$_{obsd}$						
1	1.180	–95.7	0.929	5	C(**1**)	OPBE$_{Rlt\text{-}so}$//OPBE$_{Rlt\text{-}so}$
2	1.043	–49.1	0.990	39	C(**2**)	OPBE$_{Rlt\text{-}so}$//OPBE$_{Rlt\text{-}so}$
3[c]	1.003	c	c	39	C(**2**)	OPBE$_{Rlt\text{-}so}$//OPBE$_{Rlt\text{-}so}$
4	1.177	–110.7	0.928	5	C(**1**)	BLYP$_{Rlt\text{-}so}$//OPBE$_{Rlt\text{-}so}$
5	1.086	–83.1	0.983	39	C(**2**)	BLYP$_{Rlt\text{-}so}$//OPBE$_{Rlt\text{-}so}$
6	1.321	–63.3	0.972	5	C(**1**)	BLYP$_{Rlt\text{-}so}$//MP2$_{Non}$
7	1.022	–68.5	0.980	39	C(**2**)	BLYP$_{Rlt\text{-}so}$//MP2$_{Non}$
σ^{d+p}(Te: **M**)$_{Rlt\text{-}so:r}$ versus δ(Te: **M**)$_{obsd}$						
8	0.991	–55.7	0.972	39	C(**2**)	OPBE$_{Rlt\text{-}so}$//OPBE$_{Rlt\text{-}so}$
9	0.971	–78.4	0.942	39	C(**2**)	BLYP$_{Rlt\text{-}so}$//MP2$_{Non}$
σ^{d+p}(Te: **M**)$_{Non:r}$ versus δ(Te: **M**)$_{obsd}$						
10	0.936	–101.4	0.968	39	C(**2**)	OPBE$_{Non}$//OPBE$_{Rlt\text{-}so}$
11	0.937	–148.3	0.957	39	C(**2**)	BLYP$_{Non}$//MP2$_{Non}$

[a] The constants (*a*, *b*, R^2) are the correlation constant, the *y*-intercept and the square of correlation coefficient, respectively, in $y = ax + b$. [b] Data for $TeBr_6^{2-}$ are neglected in the correlations. [c] Forced pass of the origin in the correlation with $y = ax$.

Large negative Δσδ(Te: **M**)$_{Rlt\text{-}so:r}$ values are predicted for C(**1**). While the value is extremely negative for **5** (–403 ppm), they are around –200 ppm for **2**–**4** in C(**1**). On the other hand, an extremely large positive value is predicted for **45** (540 ppm) and a large positive value is for **44** (186 ppm), although a relatively large negative value is for **46** (–122 ppm) in C(**3**). It seems difficult to predict the reliable σ^t(Te: **M**)$_{Rlt\text{-}so:r}$ values for **5** and **45**. The trend seems similar even if other two methods are applied, although better methods should be searched for or the methods should be improved.

In the case of C(**2**), magnitudes of Δσδ(Te: **M**)$_{Rlt\text{-}so:r}$ are much smaller, relative to the cases of C(**1**) and C(**3**). The magnitudes are within less than 100 ppm for most of tellurium species as shown in Figure 9. Magnitudes of Δσδ(Te: **M**)$_r$ larger than 100 ppm are as follows: *c*-$C_6H_4TeCH_2C$=O (**17**) (Δσδ(Te: **17**)$_r$ = –163 ppm), Te(C(*t*-Bu)CH)$_2$C=O (**21**) (–109 ppm), Te$(C_6H_4)_2$C=O (**22**) (–143 ppm), c-Te$(CH)_4$ (**33**) (–111 ppm) and $CF_3TeF_2CF_3$ (**40**) (159 ppm). The effect of the conjugation between Te and C=O through π-system on σ^p(Te: **M**) would be less estimated with OPBE$_{Rlt\text{-}so}$//OPBE$_{Rlt\text{-}so}$ for **M** of **17**, **21** and **22**, so would be the 6π□□□□□□ system in **33**, since the Δσδ(Te **M**)$_r$ values are negative. On the other hand, the effect of highly positively charged Te on σ^p(Te: **40**) seems overestimated with positive Δσδ(Te: **40**)$_r$, although Δσδ(Te: **M**)$_r$ are acceptable for **M** of TeF_6 (**24**) (67 ppm) and very good for Me_2TeX_2 (**29** (X = Cl) and **30** (X = Br)) and $PhTeX_2Me$ (**31** (X = Cl) and **32** (X = Br)) (–15 to –35 ppm).

□□□□σ^t(Te: **M**)$_{Rlt\text{-}so:r}$ values calculated with OPBE$_{Rlt\text{-}so}$//OPBE$_{Rlt\text{-}so}$ are plotted versus δ(Te: **M**)$_{obsd}$, separately by C(**1**), C(**2**) and C(**3**). Figure 10 shows the plots. The plots are analyzed for C(**1**) and C(**2**), assuming the linear correlations. Table 5 collects the correlations (entries 1 and 2, respectively). δ(Te: **M**)$_{obsd}$ are usually compared directly to σ^t(Te: **M**)$_{Rlt\text{-}so:r}$, in the assignment processes of ^{125}Te NMR signals. The process must correspond to the forced pass of the origin in the correlation. The treatment for C(**2**) is shown in entry 3 in Table 5, of which *a* value is equal to 1.00. The results strongly support the good applicability of σ^t(Te: **M**)$_r$ evaluated with OPBE$_{Rlt\text{-}so}$//OPBE$_{Rlt\text{-}so}$ in the assignment of δ(Te: **M**)$_{obsd}$ for usual tellurium compounds such as C(**2**). Entries 4–7 in Table 5 shows the correlations for C(**1**) and C(**2**) in the plots of σ^t(Te: **M**)$_{Rlt\text{-}so:r}$, calculated with BLYP$_{Rlt\text{-}so}$//OPBE$_{Rlt\text{-}so}$ and BLYP$_{Rlt\text{-}so}$//MP2$_{Non}$, versus δ(Te: **M**)$_{obsd}$.

The σ^{d+p}(Te: **M**)$_{Rlt\text{-}so:r}$ values calculated with OPBE$_{Rlt\text{-}so}$//OPBE$_{Rlt\text{-}so}$ and σ^{d+p}(Te: **M**)$_{Non:r}$ with OPBE$_{Non}$//OPBE$_{Rlt\text{-}so}$ are also given in Table 3 and the values with BLYP$_{Rlt\text{-}so}$//MP2$_{Non}$ are in Table S9, in the Supporting Information. Correlations for σ^{d+p}(Te: **M**)$_{Rlt\text{-}so:r}$ versus δ(Te: **M**)$_{obsd}$ for C(**2**) are given in Table 5 (entries 8 and 9) and those for σ^{d+p}(Te: **M**)$_{Non:r}$ versus δ(Te: **M**)$_{obsd}$ for C(**2**) are in Table 5 (entries 10 and 11). The R^2 values become smaller in the order of σ^t(Te: **M**)$_{Rlt\text{-}so:r}$ (0.990) > σ^{d+p}(Te: **M**)$_{Rlt\text{-}so:r}$ (0.972) > σ^{d+p}(Te: **M**)$_{Non:r}$ (0.968) if calculated with OPBE$_{Rlt\text{-}so}$//OPBE$_{Rlt\text{-}so}$ and OPBE$_{Non}$//OPBE$_{Rlt\text{-}so}$.

The (*a*, *b*, R^2) values of entries 2, 5 and 7 in Table 5 are (1.043, –49.1, 0.990), (1.086, –83.1, 0.983) and (1.022, –68.5, 0.980), respectively. The correlation obtained with OPBE$_{Rlt\text{-}so}$//OPBE$_{Rlt\text{-}so}$ seems better than other two, although the three methods could be recommended for the purpose. Both scalar-ZORA and spin-orbit ZORA relativistic effect should be considered, since the consideration of only scalar-ZORA relativistic effect seems not improve the correlations so much, relative to the case of the consideration of both effect (Table 5).

Effect of Optimized Structures on σ^t(Te: M)$_r$

The correlation for σ^t(Te: **M**)$_{Rlt\text{-}so:r}$ versus δ(Te: **M**)$_{obsd}$ must be excellent if it is analyzed as $y = ax + b$ with (*a*, *b*) = (1.00, 0.0) and R^2 very close to 1.00. What are the reasons for the deviations from the excellent case in the plot? The δ(Te: **M**)$_{obsd}$

values measured in solutions must contain solute-solute and solute-solvent interactions, whereas the theoretically predicted σ^t(Te: **M**)$_{Rlt\text{-}so;r}$ values correspond to those for single species in vacuum. Factors, other than those mentioned above, should also be examined for the better assignments of the NMR signals.

There must be some differences between optimized and observed structures. Bond distances around Te in the optimized structures are examined here, although the angular and/or torsional angular dependence of δ(Te: **M**) would affect on chemical shifts. Bond lengths around Te for some compounds optimized with OPBE$_{Rlt\text{-}so}$ are collected in Table 6, together with the observed values (□(Te-X)$_{calcd}$ and □(Te-X)$_{calcd}$, respectively, where X = C, Si, P, Te, F, Cl, Br and O). The □(Te-X)$_{calcd}$ values optimized with BLYP$_{Non}$, BLYP$_{Rlt\text{-}sc}$ and BLYP$_{Rlt\text{-}so}$ are given in Table S10 in the Supporting Information.

The Δ□(Te-X) [= □(Te-X)$_{calcd}$ – □(Te-X)$_{obsd}$] values obtained with various methods are plotted for some compounds. Figure 11 shows the results, separately by three categories of C(**1**), C(**2**) and C(**3**), similarly to the case of Figure 9. The Δ□(Te-X) values are negative for almost of the compounds examined and appear at the bottom in plots if evaluated at MP2$_{Non}$. However, the values are positive for all compounds examined and they appear at the top of the plot if calculated with BLYP$_{Rlt\text{-}so}$ and are also positive for almost of the compounds examined and appear at the next top when calculated with B3LYP$_{Non}$. The results imply that □(Te-X)$_{calcd}$ are evaluated shorter than □(Te-X)$_{obsd}$ for most of the compounds with MP2$_{Non}$, whereas □(Te-X)$_{calcd}$ are evaluated longer than □(Te-X)$_{obsd}$ with BLYP$_{Rlt\text{-}so}$ and B3LYP$_{Non}$. On the other hand, the magnitudes of Δ□(Te-X) are less than 0.01 Å for most of the compounds if evaluated with OPBE$_{Rlt\text{-}so}$ and they appear in the intermediate area between those at the MP2$_{Non}$ and B3LYP$_{Non}$ levels. The data with OPBE$_{Non}$ seem very close to those with OPBE$_{Rlt\text{-}so}$. The Δ□(Te-X) values with OPBE$_{Rlt\text{-}so}$ will be mainly discussed by classifying three categories, (i) –0.01 Å > Δ□(Te-X), (ii) –0.01 Å < Δ□(Te-X) < 0.01 Å and (iii) 0.01 Å < Δ□(Te-X). The case of (ii) is desirable.

The Δ□(Te-C) value is negligibly small for MeTeMe (**1**) (–0.0003 Å) if calculated with OPBE$_{Rlt\text{-}so}$. Fifteen Δ□(Te-X) values belong the case (ii), seven to (i) and eight to (iii), among the 30 cases. Typical cases calculated with OPBE$_{Rlt\text{-}so}$ are as follows: While Δ□(Te-P) in TeP(*i*Pr)$_3$ (**2**) satisfy the requirement of (ii) (0.002 Å), that in TePMe$_3$ (**5**) belongs to (i) (–0.027 Å). The Δ□(Te-Si) values in Te(SiMe$_3$)$_2$ (**3**) do to (iii) (0.017 Å). Indeed, a couple of Δ□(Te-C$_{eq}$) belong to (iii) (0.022 Å) and another couple of Δ□(Te-C$_{ax}$) to (ii) (–0.007 Å) in Me$_4$Te (**7**), but they belong to (ii) if the averaged value is

Table 6 Evaluate σ^t(Te: **M**)$_r$ Values at the Observed T–X Distances[a]

Compound	r(T-X)$_{opt}$ (Å)	σ^t(Te)$_r$[a] (ppm)	r(T-X)$_{obsd}$ (Å)	σ^t(Te)$_{or}$[a] (ppm)	δ(Te)$_{obsd}$[a] (ppm)	X
Te(SiMe$_3$)$_2$ (**3**)	2.531	-1053.0	2.514	-1098.4	-842	Si
TePMe$_3$ (**5**)	2.330	-916.2	2.357	-1188.8	-513.4	P
TeMe$_4$ (**7**)	2.148	-116.0	2.126	-155.8	-67.0	C
MeTeTeMe (**11**)	2.681	5.1	2.712	96.0	49	Te
PhTeTePh (**18a**)[b]	2.672	514.1	2.709	553.9	420	Te
PhTeTePh (**18b**)[b]	2.672	205.9	2.709	325.2	420	Te
c-Te(C$_6$H$_4$)$_2$CH$_2$ (**23**)	2.104	455.5	2.132	538.5	512	C
TeF$_6$ (**24**)	1.831	611.7	1.815	576.3	545	F
CF$_3$TeTeCF$_3$ (**27**)	2.225	663.5	2.181	546.1	686	C
Me$_2$TeCl$_2$ (**29**)	2.489	682.5	2.515	702.3	734	Cl
Me$_2$TeBr$_2$ (**30**)	2.654	633.3	2.683	649.0	649	Br
CF$_3$TeF$_2$CF$_3$ (**40**)	1.949	1346.7	1.974	1234.3	1187	C, F
TeCl$_6^{2-}$ (**44**)	2.568	1717.2	2.545	1489.3	1531	Cl
TeBr$_6^{2-}$ (**45**)	2.743	1888.0	2.700	1632.1	1348	Br
c-Te$_4^{2+}$ (**46**)	2.687	2542.8	2.668	2405.9	2665	Te

[a] (Te) should be read (Te: **M**). [b] σ^t(Te)$_r$ = 360 ppm and σ^t(Te)$_{or}$ = 439.6 ppm in the average.

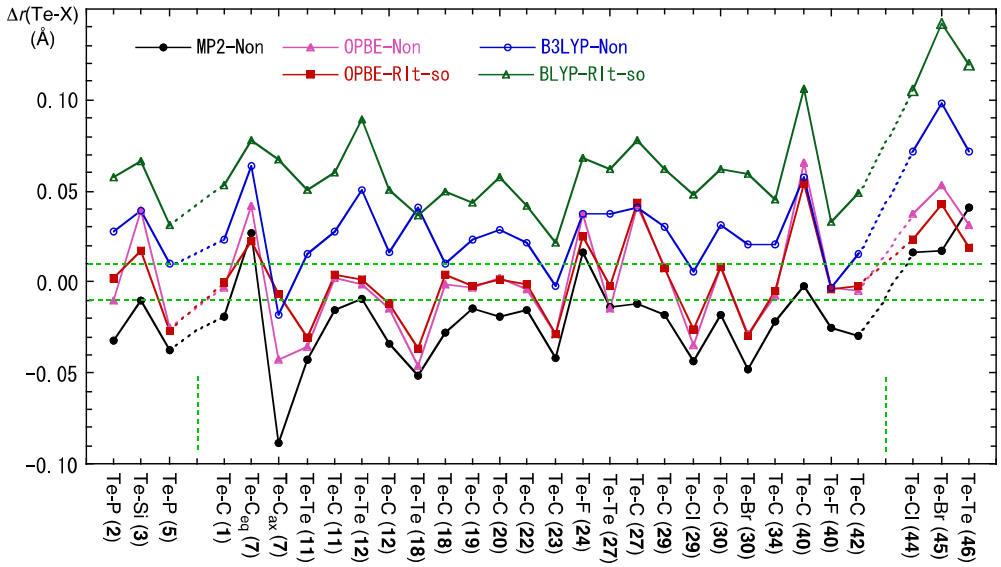

Fig. 11 Plots of Δ□(Te-X) in the structures optimized with MP2$_{Non}$, OPBE$_{Non}$, OPBE$_{Rlt\text{-}so}$, B3LYP$_{Non}$ and BLYP$_{Rlt\text{-}so}$.

examined (0.008 Å). While Δ□(Te-Te) in MeTeTeMe (**11**) (–0.031 Å) and PhTeTePh (–0.037 Å) (**18**) are in the range of (i), that in $CF_3TeTeCF_3$ (**27**) to (ii) (0.002 Å) with Δ□(Te-C) to (iii) (0.044 Å). Compounds with Δ□(Te-X) outsides of (ii) are summarized in Table 6.

The Δ□(Te-X) values with $OPBE_{Non}$ are often very close to those with $OPBE_{Rlt\text{-}so}$, as illustrated in Figure 11. Magnitudes of the differences in Δ□(Te-X) between those with $OPBE_{Non}$ and $OPBE_{Rlt\text{-}so}$ are large for **3** (X = Si: 0.0395 versus 0.0173 Å). The relativistic effect would be substantial on □(Te-Si) in **3**. While those in Δ□(Te-X) are large for **7** (X = C_{ax}: 0.0418 versus 0.0221 Å and X = C_{eq}: 0.0395 versus –0.0173 Å), that of the average value are very small (–0.0003 versus 0.0078 Å).

The Δ□(Te-X) values in the range of (i) and (iii) are tried to adjust to the observed values. The optimized distances with $OPBE_{Non}$ are very close to those with $OPBE_{Rlt\text{-}so}$. Therefore, the $OPBE_{Non}$ method is applied to the partial optimization for the adjustments, where □(Te-X) in question are fixed as the observed values. Then $\sigma^t(Te: \mathbf{M})_{Rlt\text{-}so:r}$ are evaluated with $OPBE_{Rlt\text{-}so}$ on the partially optimized structures with $OPBE_{Non}$. Table 6 collects $\sigma^t(Te: \mathbf{M})_{Rlt\text{-}so:r}$ thus evaluated for some selected species (shown by $\sigma^t(Te)_{or}$).

The $\sigma^t(Te: \mathbf{M})_{Rlt\text{-}so:r}$ values shift more high and low field as $r(T\text{-}X)_{opt}$ become shorter and longer, respectively, for the species in Table 5, except for **M** of $TePMe_3$ (**5**) and $CF_3TeF_2CF_3$ (**40**). The Te=P bond in **5** would behave differently from others in $\sigma^t(Te: \mathbf{M})$. The dependence of $\sigma^t(Te: \mathbf{M})_{Rlt\text{-}so:r}$ on the bond distance in **M** of **40** is just the opposite of that in $CF_3TeTeCF_3$ (**27**). The magnitude of $\Delta\sigma\delta(Te: \mathbf{M})_{Rlt\text{-}so:r}$ is improved for **M** of **40** (160 ppm to 47 ppm) but not for **27** (–23 to –140 ppm). Indeed, the values are much improved for **M** of $TeCl_6^{2-}$ (**44**) (186 to –42 ppm) and $TeBr_6^{2-}$ (**45**) (540 to 284 ppm), but the value for **45** after the improvement is never acceptable for the practical purpose. That for *c*-Te_4^{2+} (**46**) becomes worse (–122 to –259 ppm). The magnitudes of $\Delta\sigma\delta(Te: \mathbf{M})_{Rlt\text{-}so:r}$ are improved for 9 compounds but not for 6 compounds as a whole, if the structures with the observed distances are employed for the evaluations. It would be difficult to predict reliable $\sigma^t(Te: \mathbf{M})_{Rlt\text{-}so:r}$ for some species, such as **5** and **45**, by the methods employed above.

The $\sigma^t(Te: \mathbf{M})_{Rlt\text{-}so:r}$ values will change depending on the calculation methods, therefore, a method should be selected most suitable for the purpose or a method of wider applicability should be selected. The optimized structures can be used to predict reliable $\sigma^t(Te: \mathbf{M})_{Rlt\text{-}so:r}$, if suitable method is employed for the optimization. Observed structures may give better results. It would be recommended to employ those after partial optimization fixing some important parameters, such as bond lengths, as the observed values. The partial optimization would avoid some extreme deviations of the angular parameters in the observed structures affected from the surroundings, such as crystal packing effect.

Conclusion

The relativistic effect on σ(Z) and the components, $\sigma^d(Z)$, $\sigma^p(Z)$, $\sigma^{d+p}(Z)$ and $\sigma^{so}(Z)$ (Z = Te, Se and S), are evaluated explicitly and separately by the scalar and spin-orbit ZORA relativistic terms. The structures of various tellurium, selenium and sulfur species optimized at the MP2 level are employed for the evaluation of σ(Z). The σ(Z) values are calculated with the DFT(BLYP)-GIAO method under spin-orbit ZORA relativistic and nonrelativistic conditions with QZ4Pae. While the range of the relativistic effect on total shielding tensors for Te ($\Delta\sigma^t(Te)_{Rlt\text{-}so} = \sigma^t(Te)_{Rlt\text{-}so} - \sigma^{d+p}(Te)_{Non}$) is predicted to be –55 to 658 ppm, that for $\sigma^t(S)$ is 5 to 32 ppm, except for Me_2SBr_2 (TBP) of which $\Delta\sigma^t(S)_{Rlt\text{-}so}$ = –29 ppm. The range for $\sigma^t(Se)$ is 2 to 153 ppm. The magnitudes of the relativistic effect on $\sigma^t(Te)$, $\sigma^t(Se)$ and $\sigma^t(S)$ are about 25 : 5 : 1.

The applicability of $\sigma^t(Te: \mathbf{M})_{Rlt\text{-}so:r}$ to $\delta(Te: \mathbf{M})_{obsd}$ is examined in detail. The plot of $\sigma^t(Te: \mathbf{M})_{Rlt\text{-}so:r}$ versus $\delta(Te: \mathbf{M})_{obsd}$ is explained separately by three categories: Category 1 (C(**1**)) contains those with $\delta(Te: \mathbf{M})_{obsd:r}$ and $\sigma^t(Te: \mathbf{M})_r$ appear very high field, C(**3**) consists of the characteristic di-anionic and di-cationic species and C(**2**) forms with all compounds in Table 3 other than C(**1**) and C(**3**), which are rather usual Te species. The correlation obtained $\sigma^t(Te: \mathbf{M})_{Rlt\text{-}so:r}$ with $OPBE_{Rlt\text{-}so}$//$OPBE_{Rlt\text{-}so}$ seems better than those with $BLYP_{Rlt\text{-}so}$//$MP2_{Non}$, and $BLYP_{Rlt\text{-}so}$//$OPBE_{Rlt\text{-}so}$, although the three methods could be recommended for the purpose. The structural parameters, such as ϕ(CTeTeC) in ditellurides should be examined carefully, together with the bond length around the Te atoms. The partial optimization fixing some important parameters as the observed values would be recommended to obtain more reliable $\sigma^t(Te: \mathbf{M})_{Rlt\text{-}so:r}$.

Acknowledgements

This work was partially supported by a Grant-in-Aid for Scientific Research (Nos. 20550042, 21550046 and 23350019) from the Ministry of Education, Culture, Sports, Science and Technology, Japan. The support of the Wakayama University Original Research Support Project Grant and the Wakayama University Graduate School Project Research Grant is also acknowledged.

Notes and references

Department of Material Science and Chemistry, Faculty of Systems Engineering, Wakayama University, 930 Sakaedani, Wakayama 640-8510, Japan. Fax: +81 73 457 8253; Tel: +81 73 457 8252; E-mail: nakanisi@sys.wakayama-u.ac.jp

† Electronic Supplementary Information (ESI) available: The σ(Z) values for Z = Se and S calculated employing the structures optimized at the MP2 level are collected in Table S2 and S3, respectively. The σ(Z) values for Z = Te, Se and S calculated employing the structures optimized at the DFT (B3LYP) level are collected in Table S4–S6, respectively. Plots of $\sigma^{d+p}(Te)_{Non,r}$ and $\sigma^{d+p}(Te)_{Rlt\text{-}so,r}$ versus $\delta(Te)_{obsd}$ are depicted in

Figures S1 and S2, respectively. The full-optimized structures given by Cartesian coordinates for examined molecules and adducts. See DOI: 10.1039/b000000x/

1 (a) *Encyclopedia of Nuclear Magnetic Resonance*, eds. D. M. Grant and R. K. Harris, John Wiley Sons, New York, 1996; (b) *Nuclear Magnetic Shieldings and Molecular Structure*, ed. J. A. Tossell, Kluwer Academic Publishers, Dordrecht, 1993; (c) *Calculation of NMR and EPR Parameters; Theory and Applications*, eds. M. Kaupp, M. Bühl and V. G. Malkin, Wiley-VCH, Weinheim, 2004.

2 (a) *Introduction to Relativistic Quantum Chemistry*, eds. K. G. Dyall and K. Fægli Jr., Oxford University Press, Oxford, New York, 2007; (b) *Relativistic Quantum Chemistry: The Fundamental Theory of Molecular Science*, M. Reiher and A. Wolf, Wiley-VCH, Weinheim, 2009.

3 (a) R. Fukuda, M. Hada and H. Nakatsuji, *J. Chem. Phys.* 2003, **118**, 1015; (b) R. Fukuda, M. Hada and H. Nakatsuji, *J. Chem. Phys.* 2003, **118**, 1027; (c) S. Tanaka, M. Sugimoto, H. Takashima, M. Hada and H. Nakatsuji, *Bull. Chem. Soc. Jpn.* 1996, **69**, 953; (d) C. C. Ballard, M. Hada, H. Kaneko and H. Nakatsuji, *Chem. Phys. Lett.* 1996, **254**, 170; (e) H. Nakatsuji, M. Hada, H. Kaneko and C. C. Ballard, *Chem. Phys. Lett.* 1996, **255**, 195; (f) M. Hada, H. Kaneko and H. Nakatsuji, *Chem. Phys. Lett.* 1996, **261**, 7.

4 (a) M. Bühl, M. Kaupp, O. L. Malkina and V. G. Malkin, *J. Comput. Chem.* 1999, **20**, 91; (b) J. Konu, M. Ahlgrén, S. M. Aucott, T. Chivers, S. H. Dale, M. R. J. Elsegood, K. E. Holmes, S. L. M. James, P. F. Kelly and R. S. Laitinen, *Inorg. Chem.* 2005, **44**, 4992; (c) D. R. Urban and J. Wilcox, *J. Phys. Chem. A* 2006, **110**, 5847; (d) C. M. Widdifield and R. W. Schurko, *Conc. Magn. Reson. A* 2009, **34A**, 91.

5 (a) G. Schreckenbach and T. Ziegler, *J. Phys. Chem.* 1995, **99**, 606; (b) G. Schreckenbach and T. Ziegler, *Int. J. Quant. Chem.* 1996, **60**, 753; (c) G. Schreckenbach and T. Ziegler, *Int. J. Quant. Chem.* 1997, **61**, 899.

6 (a) S. K. Wolff and T. Ziegler, *J. Chem. Phys.* 1998, **109**, 895; (b) S. K. Wolff, T. Ziegler, E. van Lenthe and E. J. Baerends, *J. Chem. Phys.* 1999, **110**, 7689.

7 (a) E. van Lenthe, E. J. Baerends and J. G. Snijders, *J. Chem. Phys.* 1993, **99**, 4597; (b) E. van Lenthe, A. E. Ehlers and E. J. Baerends, *J. Chem. Phys.* 1999, **110**, 8943; (c) E. van Lenthe, E. J. Baerends and J. G. Snijders, *J. Chem. Phys.* 1994, **101**, 9783; (d) E. van Lenthe, J. G. Snijders and E. J. Baerends, *J. Chem. Phys.* 1996, **105**, 6505; (e) E. van Lenthe, R. van Leeuwen, E. J. Baerends and J. G. Snijders, *Int. J. Quantum Chem.* 1996, **57**, 281.

8 J. R. Yates, C. J. Pickard, M. C. Payne and F. Mauri, *J. Chem. Phys.* 2003, **118**, 5746.

9 Based on the second-order perturbation theory at the level of the HF and single-excitation CI approximation, $\sigma^{p}_{i\rightarrow a}$ on a resonance nucleus N is shown to be proportional to reciprocal orbital energy gap $(\varepsilon_a-\varepsilon_i)^{-1}$. $\sigma^{p}_{zz}(N)$ are approximately given by eq 1, where ψ_k is the k-th orbital function, $\hat{}L_{z,N}$ is orbital angular momentum around the resonance nucleus, and r_N is the distance from the nucleus N.

10 (a) W. McFarlane and R. J. Wood, *J. Chem. Soc., Dalton Trans.* 1972, 1397; (b) H. Iwamura and W. Nakanishi, *J. Syn. Org. Chem. Jpn.* 1981, **39**, 795; (c) *The Chemistry of Organic Selenium and Tellurium Compounds*, *Vol. 1*, eds. S. Patai and Z. Rappoport, Wiley, New York, 1986, Ch. 6; (d) *Compilation of Reported ^{77}Se NMR Chemical Shifts*, eds. T. M. Klapötke and M. Broschag, Wiley, New York, 1996; (e) H. Duddeck, *Prog. Nucl. Magn. Reson. Spectrosc.* 1995, **27**, 1.

11 (a) S. Hayashi and W. Nakanishi, *J. Org. Chem.* 1999, **64**, 6688; (b) W. Nakanishi and S. Hayashi, *Chem. Lett.* 1998, 523; (c) W. Nakanishi and S. Hayashi, *J. Phys. Chem. A* 1999, **103**, 6074; (d) W. Nakanishi, S. Hayashi and M. Hada, *Chem. Eur. J.* 2007, **13**, 5282; (e) W. Nakanishi, S. Hayashi, D. Shimizu and M. Hada, *Chem. Eur. J.* 2006, **12**, 3829; (f) S. Hayashi and W. Nakanishi, *Bioinorganic Chemistry and Applications*, 2006, doi:10.1155/BCA/2006/79327.

12 (a) W. Nakanishi, S. Hayashi, K. Narahara, D. Yamaki and M. Hada, *Chem. Eur. J.* 2008, **14**, 7278; (b) W. Nakanishi, S. Hayashi, K. Narahara and M. Hada, *Chem. Eur. J.* 2008, **14**, 9647.

13 (a) A. D. Becke, *J. Chem. Phys.* 1993, **98**, 5648; (b) C. Lee, W. Yang and R. G. Parr, *Phys. Rev. B* 1988, **37**, 785; (c) A. D. Becke, *Phys. Rev. A* 1988, **38**, 3098.

14 W. Nakanishi, S. Hayashi, Y. Katsura and M. Hada, *J. Phys. Chem. A* 2011, **115**, 8721.

15 Y. Ruiz-Morales, G. Schreckenbach and T. Ziegler, *J. Phys. Chem. A* 1997, **101**, 4121.

16 G. te Velde, F. M. Bickelhaupt, S. J. A. van Gisbergen, C. Fonseca Guerra, E. J. Baerends, J. G. Snijders and T. Ziegler, *J. Comput. Chem.* 2001, **22**, 931.

17 C. Fonseca Guerra, J. G. Snijders, G. te Velde and E. J. Baerends, *Theor. Chem. Acc.* 1998, **99**, 391.

18 ADF2013, SCM, *Theoretical Chemistry*, Vrije Universiteit, Amsterdam (The Netherlands), http://www.scm.com: E. J. Baerends, T. Ziegler, J. Autschbach, D. Bashford, A. Bérces, F. M. Bickelhaupt, C. Bo, P. M. Boerrigter, L. Cavallo, D. P. Chong, L. Deng, R. M. Dickson, D. E. Ellis, M. van Faassen, L. Fan, T. H. Fischer, C. Fonseca Guerra, M. Franchini, A. Ghysels, A. Giammona, S. J. A. van Gisbergen, A. W. Götz, J. A. Groeneveld, O. V. Gritsenko, M. Grüning, S. Gusarov, F. E. Harris, P. van den Hoek, C. R. Jacob, H. Jacobsen, L. Jensen, J. W. Kaminski, G. van Kessel, F. Kootstra, A. Kovalenko, M. V. Krykunov, E. van Lenthe, D. A. McCormack, A. Michalak, M. Mitoraj, S. M. Morton, J. Neugebauer, V. P. Nicu, L. Noodleman, V. P. Osinga, S. Patchkovskii, M. Pavanello, P. H. T. Philipsen, D. Post, C. C. Pye, W. Ravenek, J. I. Rodríguez, P. Ros, P. R. T. Schipper, G. Schreckenbach, J. S. Seldenthuis, M. Seth, J. G. Snijders, M. Solà, M. Swart, D. Swerhone, G. te Velde, P. Vernooijs, L. Versluis, L. Visscher, O. Visser, F. Wang, T. A. Wesolowski, E. M. van Wezenbeek, G. Wiesenekker, S. K. Wolff, T. K. Woo, A. L. Yakovlev.

19 (a) K. Wolinski, J. F. Hinton and P. Pulay, *J. Am. Chem. Soc.* 1990, **112**, 8251; (b) K. Wolinski and A. Sadlej, *Mol. Phys.* 1980, **41**, 1419; (c) R. Ditchfield, *Mol. Phys.* 1974, **27**, 789; (d) R. McWeeny, *Phys. Rev.* 1962, **126**, 1028; (e) F. London, *J. Phys. Radium, Paris* 1937, **8**, 397.

20 E. van Lenthe and E. J. Baerends, *J. Comput Chem.* 2003, **24**, 1142.

21 The absolute basis set error of 0.03 kcal mol^{-1} in the average has been reported in the DFT calculation of the valence spinor energies of the neutral atoms of H (Z = 1) to E118 (Z = 118), with the QZ4Pae quality, under the scalar ZORA relativistic conditions. This average absolute basis set error increases to about 1 kcal mol^{-1} for

the TZ2Pae quality, and to approximately 4 kcal mol^{-1} for the DZ (double zeta) quality.

22 D. B. Chesnut, *Chem. Phys. Lett.* 1995, **246**, 235.

23 Gaussian 03, Revision E.01, M. J. Frisch, G. W. Trucks, H. B. Schlegel, G. E. Scuseria, M. A. Robb, J. R. Cheeseman, J. A. Montgomery, Jr., T. Vreven, K. N. Kudin, J. C. Burant, J. M. Millam, S. S. Iyengar, J. Tomasi, V. Barone, B. Mennucci, M. Cossi, G. Scalmani, N. Rega, G. A. Petersson, H. Nakatsuji, M. Hada, M. Ehara, K. Toyota, R. Fukuda, J. Hasegawa, M. Ishida, T. Nakajima, Y. Honda, O. Kitao, H. Nakai, M. Klene, X. Li, J. E. Knox, H. P. Hratchian, J. B. Cross, V. Bakken, C. Adamo, J. Jaramillo, R. Gomperts, R. E. Stratmann, O. Yazyev, A. J. Austin, R. Cammi, C. Pomelli, J. W. Ochterski, P. Y. Ayala, K. Morokuma, G. A. Voth, P. Salvador, J. J. Dannenberg, V. G. Zakrzewski, S. Dapprich, A. D. Daniels, M. C. Strain, O. Farkas, D. K. Malick, A. D. Rabuck, K. Raghavachari, J. B. Foresman, J. V. Ortiz, Q. Cui, A. G. Baboul, S. Clifford, J. Cioslowski, B. B. Stefanov, G. Liu, A. Liashenko, P. Piskorz, I. Komaromi, R. L. Martin, D. J. Fox, T. Keith, M. A. Al-Laham, C. Y. Peng, A. Nanayakkara, M. Challacombe, P. M. W. Gill, B. Johnson, W. Chen, M. W. Wong, C. Gonzalez and J. A. Pople, Gaussian, Inc., Wallingford CT, 2004.

24 (a) T. Koga, S. Yamamoto, T. Shimazaki and H. Tatewaki, *Theor. Chem. Acc.* 2002, **108**, 41; (b) M. Sekiya, T. Noro, Y. Osanai and T. Koga, *Theor. Chem. Acc.* 2001, **106**, 297.

25 For the 6-311G(3d) basis sets see, (a) R. C. Binning Jr. and L. A. Curtiss, *J Comput. Chem.* 1990, **11**, 1206; (b) L. A. Curtiss, M. P. McGrath, J.-P. Blaudeau, N. E. Davis, R. C. Binning, Jr. and L. Radom, *J. Chem. Phys.* 1995, **103**, 6104; (c) M. P. McGrath and L. Radom, *J. Chem. Phys.* 1991, **94**, 511. For the diffuse functions (+ and ++) see, T. Clark, J. Chandrasekhar, G. W. Spitznagel and P. von R. Schleyer, *J. Comput. Chem.* 1983, **4**, 294.

26 M. Hdada, J. Wan, R. Fukuda and H. Nakatsuji, *J. Comput. Chem.* 2001, **22**, 1502.

27 Y. Ruiz-Morales, G. Schreckenbach and T. Ziegler, *J. Phys. Chem.* 1997, **101**, 4121.

28 C. J. Jameson, A. K. Jameson, *Chem. Phys. Lett.* 1987, **135**, 254.

29 H. C. E. McFarlane and W. McFarlane, *Multinuclear NMR*, ed. J. Mason, Plenum: New York, 1987, pp. 417-435.

30 C. Rodger, N. Sheppard, C. McFarlane and W. McFarlane, *NMR and the Periodic Table*, eds. R. K. Harris and B. E. Mann, Academic Press, 1978, pp. 383-419.

31 N. Kuhn, G. Henkel, H. Schumman and R. Fröhlich, *Z. Naturforsh.* 1990, **45b**, 1010.

32 C. H. W. Jones, R. D. Sharma and S. P. Taneja, *Can. J. Chem.* 1986, **64**, 980.

33 J. Vaara, K. Ruud and O. Vahtras, *J. Chem. Phys.* 1999, **111**, 2900.

34 H. C. McFarlane and W. McFarlane, *J. Chem. Soc., Dalton Trans.* 1973, 2416.

35 N. Kuhn, G. Henkel and T. Kratz, *Chem. Ber.* 1993, **126**, 2047.

36 R. W. Gedridge, Jr., D. C. Harris, K. T. Higa and R. A. Nissan, *Organomet.* 1989, **8**, 2817.

37 D. H. O'Brien, N. Dereu, C.-K. Huang, K. J. Irgolic and F. F. Knapp, Jr., *Organomet.* 1983, **2**, 305.

38 N. Zumbulyadis and H. J. Gysling, *J. Organomet. Chem.* 1980, **192**, 183.

39 M. V. Lakshmikantham, M. P. Cava, W. H. H. Günther, P. N. Nugara, K. A. Belmore, J. L. Atwood and P. Cragg, *J. Am Chem. Soc.* 1993, **115**, 885.

40 D. H. O'Brien, N. Dereu, R. A. Grigsby, K. J. Irgolic and F. F. Knapp, Jr. *Organomet.* 1982, **1**, 513.

41 H. Fujiwara, T. Ninoi, R. Akasaka, T. Erata and N. Furukawa, *Tetrahedron Lett.* 1991, **32**, 4537.

42 M. R. Detty, W. C. Lenhart, P. G. Gassman and M. R. Callstrom, *Organometallics* 1989, **8**, 861.

43 W. Lohner and K. Praefcke, *J. Organomet. Chem.* 1981, **208**, 39.

44 E. W. Abel, M. A. Beckett, K. G. Orrell, V. Sik, D. Stephenson, H. B. Singh and N. Sudha, *Polyhedron*, 1988, **7**, 1169.

45 K. Laali, H. Y. Chen and R. J. Gerzina, J. Org. Chem. 1987, 52, 4126.

46 G. A. Kalabin, R. B. Valeev and D. F. Kushnarev, *Zh. Org. Kim.* 1981, **17**, 947.

47 T. Drakenberg, F. Fringuelli, S. Gronowitz, A.-B. Hörnfeldt, I. Johnson and A. Taticchi, *Chem. Scr.* 1976, **10**, 139.

48 R. W. Gedridge, Jr., D. C. Harris, K. T. Higa and R. A. Nissan, *Organomet.* 1989, **8**, 2817.

49 H. Duddeck, *Sulfur, Selenium, & Tellurium NMR*, in *Encyclopedia of Nuclear Magnetic Resonance*, eds. D. M. Grant, R. K. Harris, John Wiley Sons, New York, 1996, pp. 4623-4636.

50 J. E. Drake, L. N. Khasrou, A. G. Mislankar and R. Ratnani, *Inorg. Chem.* 1994, **33**, 6154.

51 N. L. M. Dereu and R. A. Zingaro, *J. Organomet. Chem.* 1981, **212**, 141.

52 D. C. Harris, R. A. Nissan and K. T. Higa, *Inorg. Chem.* 1987, **26**, 765.

53 T. G. Back, D. Kuzma and M. Parvez, *J. Org. Chem.* 2005, **70**, 9230.

54 W. *Z.* Gombler, *Naturforsch. B* 1981, **36B**, 535.

55 M. Minoura, T. Kawashima and R. Okazaki, *J. Am. Chem. Soc.* 1993, **115**, 7019.

56 R. Boese, A. Haas and C. Limberg, *J. Chem., Soc., Chem. Commun.* **1991**, 1378.

57 R. Blom, A. Haaland and R. Seip, *Acta Chem. Scand.* 1983, **A37**, 595.

58 C. R. Lassigne and E. J. Wells, *J. Chem. Soc., Chem. Commun.* 1978, 956.

59 Figure S7 draws the C_{2v}, C_4 and T_d structures of **7**, optimized with MP2$_{Non}$. Table S11 collects the $\sigma^{\square}(\mathrm{Te})_{\mathrm{Rlt\text{-}so:}r}$ values for TeF_4 (C_{2v}), TeF_4 (C_{4v}), TeF_4 (T_d), **7** (C_{2v}), **7** (C_4) and **7** (T_d), together with some structural data and the relative contributions. The T_d structures are estimated to be so unstable, therefore, they need not be considered in $\sigma^{\square}(\mathrm{Te})_{\mathrm{Rlt\text{-}so:}r}$. The $\sigma^{\square}(\mathrm{Te})_{\mathrm{Rlt\text{-}so:}r}$ values of TeF_4 (C_{2v}), TeF_4 (C_4), **7** (C_{2v}) and **7** (C_4) are predicted to be 1651, 1532, –116, and –242 ppm, respectively. TeF_4 (C_{2v}) and **7** (C_4) are predicted to contribute predominantly, relative to the case of TeF_4 (C_4) and **7** (C_{2v}), respectively. However, $\sigma^{\square}(\mathrm{Te})_{\mathrm{Rlt\text{-}so:}r}$ of **7** (C_{2v}) seems to explain $\delta(\mathrm{Te})_{obsd}$ of **7** (–67 ppm) better than that of **7** (C_4). **7** (C_{2v}) would be predominantly in the solution, maybe due to the solvent effect.

Journal Name RSCPublishing

ARTICLE

Graphical contents entry:

The relativistic effect on σ(Te), σ(Se) and σ(S) is evaluated separately by scalar and spin-orbit terms for various tellurium, selenium, and sulfur species. The applicability of $\sigma^{t}(Te)_{Rlt\text{-}so}$ to analyze $\delta(Te)_{obsd}$ and the trend in the nuclei are discussed.

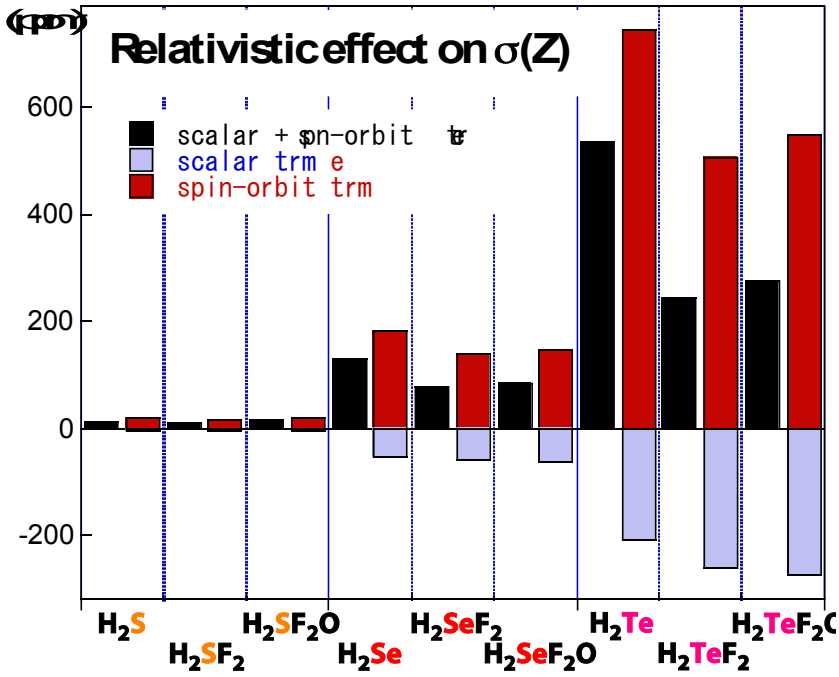

Keywords:

ab initio calculations · absolute magnetic shielding tensors · NMR chemical shifts · relativistic effect · tellurium · ZORA